Preprints.org

Article

Not peer-reviewed version

Genesis of the Dongtangzi Zn-Pb Deposit of the Fengxian-Taibai Ore Cluster in West Qinling, China: Constraints from Rb-Sr and Sm-Nd Geochronology, and In-Situ S-pb Isotopes

Qiaoqing Hu , Yitian Wang * , Shaocong Chen , Ran Wei , Xielu Liu , Junchen Liu , Ruiting Wang , Weihong Gao , Changan Wang , Minjie Tang , Wentang Wu , Qiaoqing Hu

Posted Date: 11 January 2024

doi: 10.20944/preprints202401.0877.v1

Keywords: Rb-Sr and Sm-Nd isotopic dating; In-situ S-Pb isotopes; Ore genesis; Zn-Pb deposit; Dongtangzi; West Qinling orogen

Preprints.org is a free multidiscipline platform providing preprint service that is dedicated to making early versions of research outputs permanently available and citable. Preprints posted at Preprints.org appear in Web of Science, Crossref, Google Scholar, Scilit, Europe PMC.

Copyright: This is an open access article distributed under the Creative Commons Attribution License which permits unrestricted use, distribution, and reproduction in any medium, provided the original work is properly cited.

Preprints (www.preprints.org) | NOT PEER-REVIEWED | Posted: 11 January 2024 doi:10.20944/preprints202401.0877.v1

Disclaimer/Publisher's Note: The statements, opinions, and data contained in all publications are solely those of the individual author(s) and contributor(s) and not of MDPI and/or the editor(s). MDPI and/or the editor(s) disclaim responsibility for any injury to people or property resulting from any ideas, methods, instructions, or products referred to in the content.

Article

Genesis of the Dongtangzi Zn-Pb Deposit of the Fengxian-Taibai Ore Cluster in West Qinling, China: Constraints from Rb-Sr and Sm-Nd Geochronology, and In-Situ S-Pb Isotopes

Qiaoqing Hu [a], Yitian Wang [a,*], Shaocong Chen [a], Ran Wei [a], Xielu Liu [b], Junchen Liu [c], Ruiting Wang [d], Weihong Gao [d], Changan Wang [e], Minjie Tang [e] and Wentang Wu [e]

[a] MNR Key Laboratory of Metallogeny and Mineral Assessment, Institute of Mineral Resources, Chinese Academy of Geological Sciences, Beijing 100037, China; huqiaoqing@cags.ac.cn
[b] Beijing Institute of Exploration Engineering, Beijing, 100083, China
[c] Collaborative Innovation Center for Exploration of Nonferrous Metal Deposits and Efficient Utilization of Resources by the Province and Ministry, Guilin University of Technology, Guilin, 541004, China
[d] Northwest Nonferrous Geological and Mining Group Co., Ltd., Xi'an 710054, Shaanxi, China
[e] Baoji No.717 Corps Limited of Northwest Nonferrous Geological and Mining Group, Baoji 721015, Shaanxi, China
* Correspondence: Yitian Wang, MNR Key Laboratory of Metallogeny and Mineral Assessment, Institute of Mineral Resources, Chinese Academy of Geological Sciences, Beijing 100037, China. Email address: wyt69@263.net

Abstract: The Dongtangzi large Zn-Pb deposit is located in the southwest of the Fengxian-Taibai (abbr. Fengtai) ore cluster in the west Qinling orogen, whose origin has been controversial, positing diverse genesis mechanisms such as sedimentary-exhalative (SEDEX), sedimentary-reformed, and epigenetic hydrothermal type. In this work, based on detailed observation and systematic study on ore geology, the results of high-precision Rb-Sr isotopic dating on sulfides of the main orebody and Sm–Nd isotopic dating on associated carbonates have been carried out, which yield isochron ages of 211.6 ± 2.6 Ma and 211 ± 4 Ma, respectively. In-situ S-Pb isotopic studies show that the ore related sulfides display a narrow range of $\delta^{34}S$ values from 1.1 ‰ to 10.2 ‰, with $^{206}Pb/^{204}Pb$, $^{207}Pb/^{204}Pb$ and $^{208}Pb/^{204}Pb$ ratios of 18.07 to 18.27, 15.64 to 15.66, and 38.22 to 38.76, respectively. While the pyrite of sedimentary period and the granite porphyry dike have $\delta^{34}S$ values vary from 15.8 to 21.4‰, and from 2.1 to 4.3‰ (with $^{206}Pb/^{204}Pb$ ratios of 18.09 to 18.10, $^{207}Pb/^{204}Pb$ ratios of 15.59 to 15.61, and $^{208}Pb/^{204}Pb$ ratios of 38.17 to 38.24) respectively. Combining the regional geology, we propose that the Dongtangzi Zn-Pb deposit is the product of multi-stage epigenetic hydrothermal fluid processes, driven by late Triassic regional tectono-magmatic activities in regional extensional regime, with metallic materials originate from a mixture of Triassic magmatic processes and metamorphic basement.

Keywords: Rb-Sr and Sm-Nd isotopic dating; In-situ S-Pb isotopes; Ore genesis; Zn-Pb deposit; Dongtangzi; West Qinling orogen

1. Introduction

The Fengxian–Taibai (abbr. "Fengtai") ore cluster in the Shaanxi Province, located in the west Qinling orogenic belt, China, is an important part of the giant Qinling Pb-Zn-Au metallogenic belt. Several large and medium-sized Zn-Pb deposits are present, including, from west to east, the Fengya, Yindongliang, Qiandongshan-Dongtangzi, Bafangshan-Erlihe, and Yinmusi deposits, along with many small-sized deposits and occurrences. Besides, there are two large Au deposits of the Baguamiao and Shuangwang, along with many small-sized Au deposits, and several small Cu deposits. The total reserve is over 5 Mt Pb+Zn and more than 200 t gold in the ore cluster (Wang R.T. et al., 2007; Li, 2008). The large Dongtangzi Zn-Pb deposit, located in the southwest of the Fengtai ore cluster (Figure 1c), contains over 1.5 Mt Pb+Zn, with an average grade of 7.7 wt% Zn and 1.7 wt% Pb (Wu et al., 2016). The Dongtangzi Zn-Pb deposit was discovered in the late 1950s, which was formerly

© 2024 by the author(s). Distributed under a Creative Commons CC BY license.

Preprints (www.preprints.org) | NOT PEER-REVIEWED | Posted: 11 January 2024 doi:10.20944/preprints202401.0877.v1

known as the Qiandongshan deposit. With the deepening of the exploration work, around the year 2002, the newly discovered concealed west part of the main ore body is called the Dongtangzi mine section. After the year 2004, the two mine sections were merged into one company, collectively called the Dongtangzi Zn-Pb deposit. The previous research work was mainly done on the Qiandongshan mine section, while less work has been done on the Dongtangzi mine section. Since the 1980s, extensive investigations into the Dongtangzi Zn-Pb deposit have been done into its geological characteristics and ore-controlling structures (Zhang, 1986; Wang J.L. et al., 1996; Wu W.T. et al., 2015; Wu X.D. et al., 2016; Wang Y.T. et al., 2020a), stable isotope and trace elements geochemistry (Fang, 1999a, 1999b; Huang et al., 2003; Ren et al., 2014; Zhang et al., 2020), and ore genesis (Li, 1986; Yang X.K. et al., 1991; Li et al., 1992; Qi and Li, 1993; Wang J.L. et al., 1996; Zhang et al., 2018; Zhang et al., 2020; Wang et al., 2021; Shi et al., 2022). Despite decades of research, the origin of the ore remains contentious.

Prevailing perspectives (e.g., Zhang and Wang., 1988; Qi and Li, 1993; Wang J.L. et al., 1996; Wang D.S. et al., 2009; Wang R.T. et al., 2011) believed that it is a SEDEX deposit developed in Devonian or a sedimentary-reformed deposit. Conversely, proponents of the epigenetic hydrothermal ore deposit theory (Wang Y.T. et al., 2009, 2011, 2013, 2020a, 2021; Hu et al., 2015, 2020; Zhang et al., 2018; Shi et al., 2022) contend that it is a product of Triassic tectonic-hydrothermal processes. Due to the lack of a precise geochronology data and comprehensive isotopic geochemistry studies, especially the lack of in-situ technique analysis, the metallogenic processes of the Dongtangzi Zn-Pb deposit remains poorly understood. Therefore, this study presents a comprehensive recognition of its deposit geology, along with Rb-Sr and Sm-Nd geochronology and in-situ S-Pb isotopic studies, aiming to enhance the comprehension of the ore genesis. The new results in this study, provide valuable information about the timing of Zn-Pb mineralization and the source of ore-forming materials, and allow us to refine the origin of the Dongtangzi Zn-Pb deposit, which will be an essential factor for understanding the Zn-Pb metallogeny throughout the entire Fengtai ore cluster and the West Qinling Zn-Pb belt.

2. Regional Geology

The Qinling orogen was formed from the convergence and collision of the North China block and the Yangtze block (Figure 1a), which is a multi-stage composite orogenic belt composed of two suture zones and three tectonic units (Zhang et al., 2004). The northern suture zone is the Early Silurian Shangdan suture (Figure 1b), and the southern is the Late Triassic Mianlue suture (Figure 1b). The three tectonic units are, from north to south, the south margin of the North China block and the North Qinling belt, the South Qinling belt, and the north margin of the Yangtze block (Zhang et al., 2004). The Fengtai ore cluster is located in the middle-west of the South Qinling belt (Figure 1c), which is bordered by the NWW-trending faults of the Xiangzihe—Huangbaiyuan fault (F_1, part of the Shangdan suture) in the north and the Jiudianliang—Jiangkou fault (F_5) in the south (Figure 1c). There are three NWW-trending faults inside the ore cluster called Xiushiyan—Guanyinxia (F_2), Wangjialeng—Erlangba (F_3) and Daohuigou—Zheliyuan (F_4) faults (Figure 1c). The basic tectonic framework of the ore cluster is a compound fold with well-developed secondary folds and faults. The tectonic style is a large-scale transpressional strike-slip duplex system resulted from regional sinistral strike-slip faulting (Wang Y.T. et al., 2009, 2018).

Preprints (www.preprints.org) | NOT PEER-REVIEWED | Posted: 11 January 2024 doi:10.20944/preprints202401.0877.v1

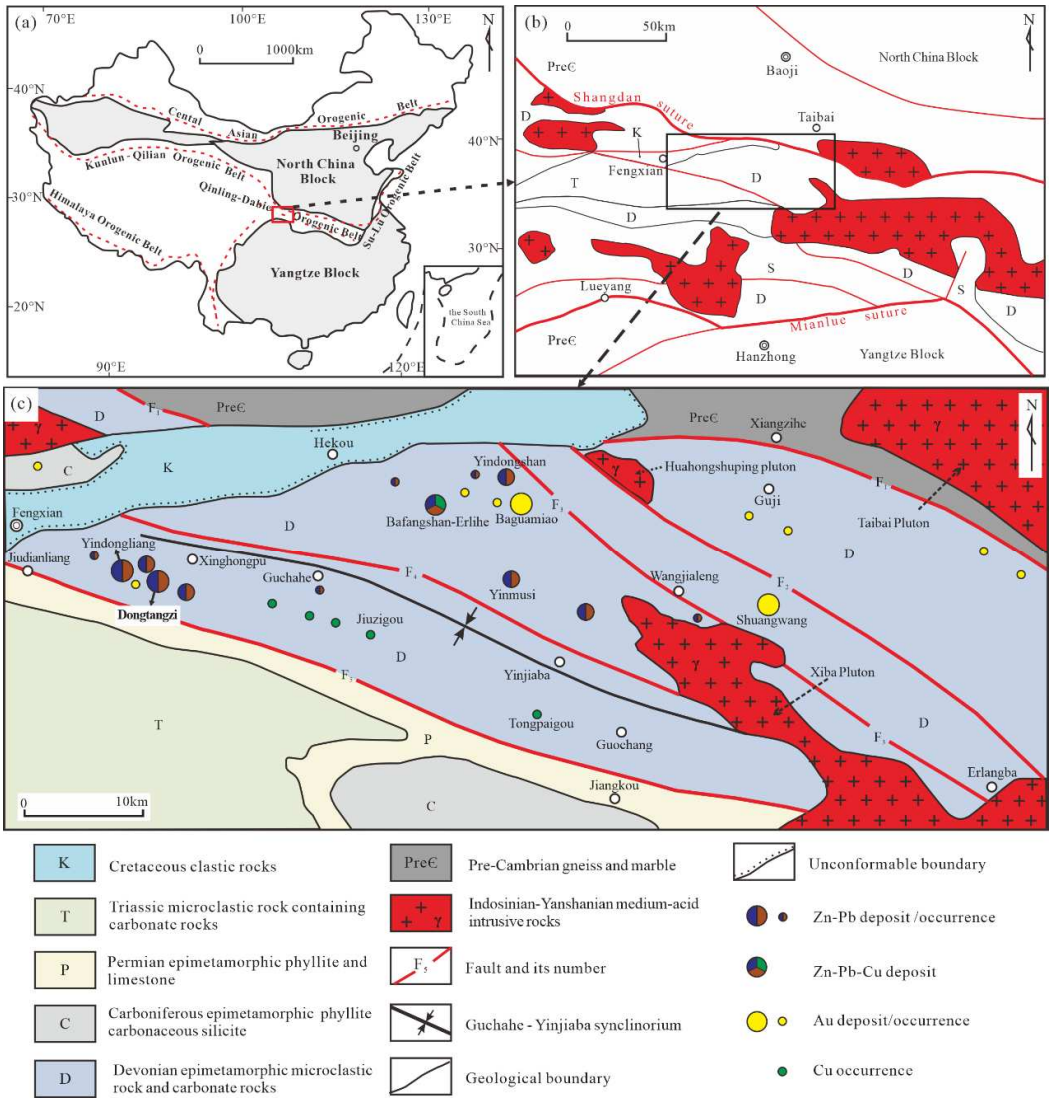

Figure 1. Sketch map of tectonic units of China (a) and west Qinling orogenic belt (b), along with a geological map of the Fengxian-Taibai ore cluster (c) (modified from Wang X. et al. 1996; Hu Q.Q. et al., 2020). Notes: F_1: Xiangzihe-Huangbaiyuan Fault (Shang-Dan suture zone); F_2: Xiushiyan-Guanyinxia Fault; F_3: Wangjialeng-Erlangba Fault; F_4: Daohuigou-Zheliyuan Fault; F_5: Jiudianliang-Jiangkou Fault.

The stratigraphic sequence of the Fengtai ore cluster is comprised of the Middle-Upper Devonian epimetamorphic littoral-neritic facies clastic and carbonate rocks (Figure 1c). This vertical succession comprises, from bottom to top, fine clastic rocks and metasandstone of the Middle Devonian Macaogou Formation (D_2m), followed by carbonate rocks of the Middle Devonian Gudaoling Formation (D_2g), epimetamorphic clastic-carbonate rocks of the Upper Devonian Xinghongpu Formation (D_3x), and fine clasolite of the Upper Devonian Jiuliping Formation (D_3j). Around the periphery of the ore cluster, the high grade metamorphic pararock and volcanics of the Proterozoic Qinling Group (Pt_1q) and Danfeng Group (Pt_1d) appear to the north, the carbonate and clastic rocks of the Lower Carboniferous (C_1) and breccia with siltstone of the Lower Cretaceous (K_1) to the northwest (Figure 1c), the marine carbonate rocks with continental clastic rocks of the Carboniferous (C), and limestone of the Lower Triassic Liufengguan Group (T_1l) to the southwest (Figure 1c).

Intense Triassic magmatism was well developed in the ore cluster. The Xiba intermediate-felsic pluton, trending NWW, is positioned to the southeast of the cluster (Figure 1c), comprising medium-fine grained granodiorite, monzogranite, quartz diorite, and tonalite, with transitional contact

Preprints (www.preprints.org) | NOT PEER-REVIEWED | Posted: 11 January 2024 doi:10.20944/preprints202401.0877.v1

relations. The small Huahongshuping granodioritic intrusive stock is located in the north (Figure 1c). In addition, numerous dikes of diorite, granite porphyry and lamprophyre commonly develop over the ore cluster (mainly concentrated adjacent to the Pb-Zn and Au deposits), filling the NE- or NWW-trending faults, with a thickness of tens of centimeters to several meters.

3. Ore deposit geology

3.1. Structures

The "M"-shaped Qiandongshan-Dongtangzi brachy-anticline is the principle ore-hosting structure, with the anticlinal axis plane strike range from 275° to 285° (Figure 2). The hinge of the anticline pitches toward west, with the plunge angles ranging from 27° to 37° (Tang, 2013). There are EW-, NW- and NE-trending faults in the mine area. The EW-trending faults are largest in scale, developed mostly in the interface between Gudaoling formation and Xinghongpu formation, belonging to reverse faults (Figure 2). The NW- and NE-trending faults are small in scale and large in number, belonging to the "X" type conjugate shear faults formed under regional shearing events, cutting through the main ore body with small fault displacement.

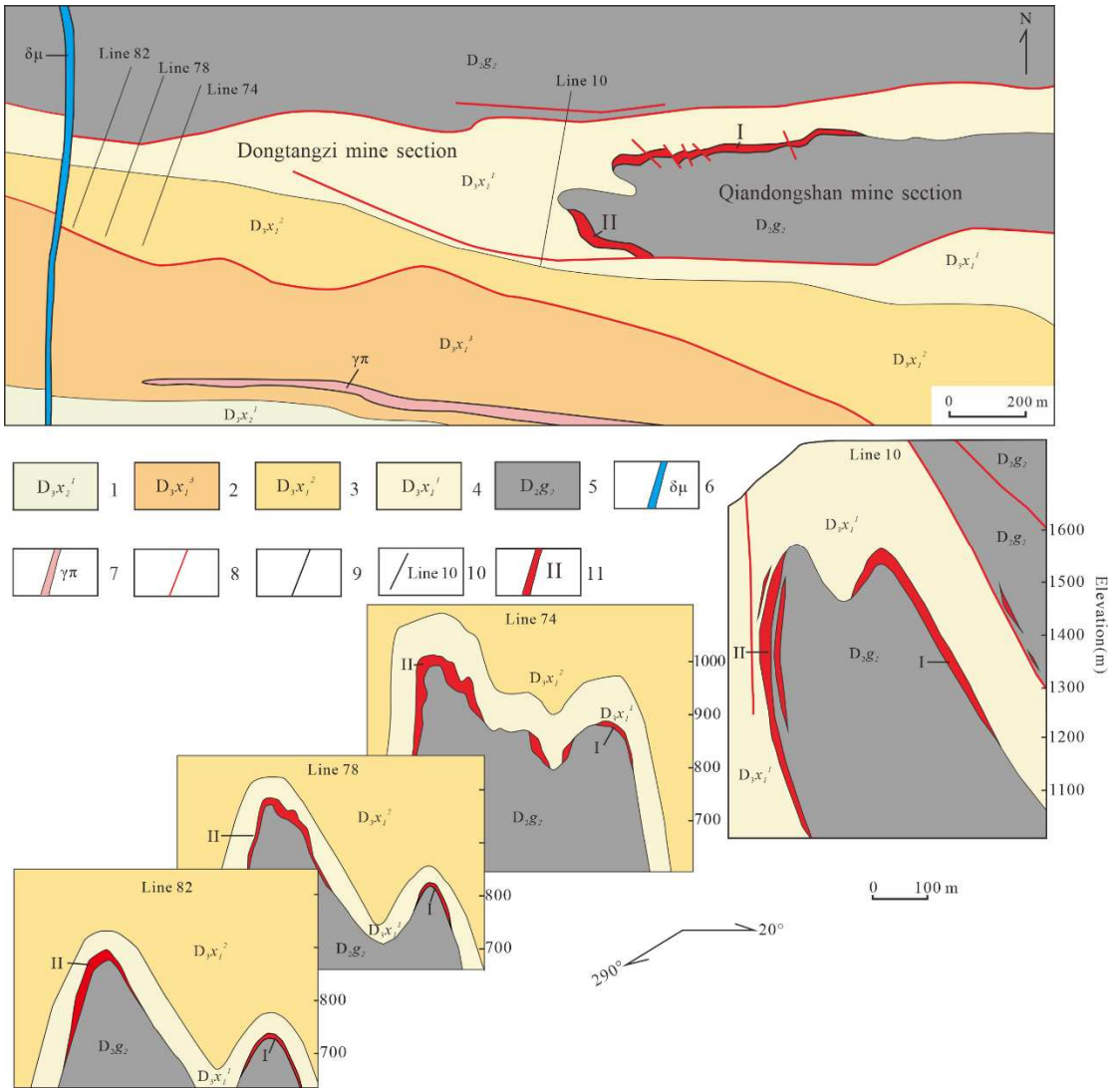

Figure 2. Geological map and composite cross sections of the Dongtangzi Zn-Pb deposit (after Qi et al., 1993; Tang, 2013; Wu et al., 2016; Wang et al., 2023) Note: 1. Chlorite sericite phyllite, the first layer of the second lithologic section of Upper Devonian Xinghongpu Fm. ($D_3x_2^1$); 2. The third layer of the first lithologic section of Upper Devonian Xinghongpu Fm. ($D_3x_1^3$); 3. The second layer of the first lithologic section of Upper Devonian Xinghongpu Fm. ($D_3x_1^2$); 4. First layer of the first lithologic

Preprints (www.preprints.org) | NOT PEER-REVIEWED | Posted: 11 January 2024 doi:10.20944/preprints202401.0877.v1

section of Upper Devonian Xinghongpu Fm. ($D_3x_1^1$); 5. The upper section of the Upper Devonian Gudaoling Fm. (D_2g_2); 6. Diorite porphyry dike; 7. Granite porphyry dike; 8. Fault; 9. Geological boundary; 10. Prospecting line and its number; 11. Zn-Pb orebody and its number.

3.2. Rocks

The strata within the mine area contains the upper section of the Gudaoling Formation of middle Devonian (D_2g_2) and the the Xinghongpu Formation of middle Devonian (D_3x) (Figure 2). The EW-striking upper section of the Gudaoling Formation, consisting of microcrystalline biolithite and carbonaceous microcrystalline limestone, silicified intensively in the top by meters to tens of meters in thickness, hosts the main orebody. The first lithologic section of the Xinghongpu Formation consists of ferrodolomitic phyllite with sericite phyllite and thin layer of carbonaceous limestone at the bottom, ferrodolomitic phyllite with thin layer of limestone and silty sericite phyllite in the middle, and carbonaceous calcareous sericite phyllite with thin layer of carbonaceous biolithite at the top. The second lithologic section of the Xinghongpu Formation consists mainly of chlorite sericite phyllite, with less ferrodolomitic sericite phyllite at the bottom (Figure 3).

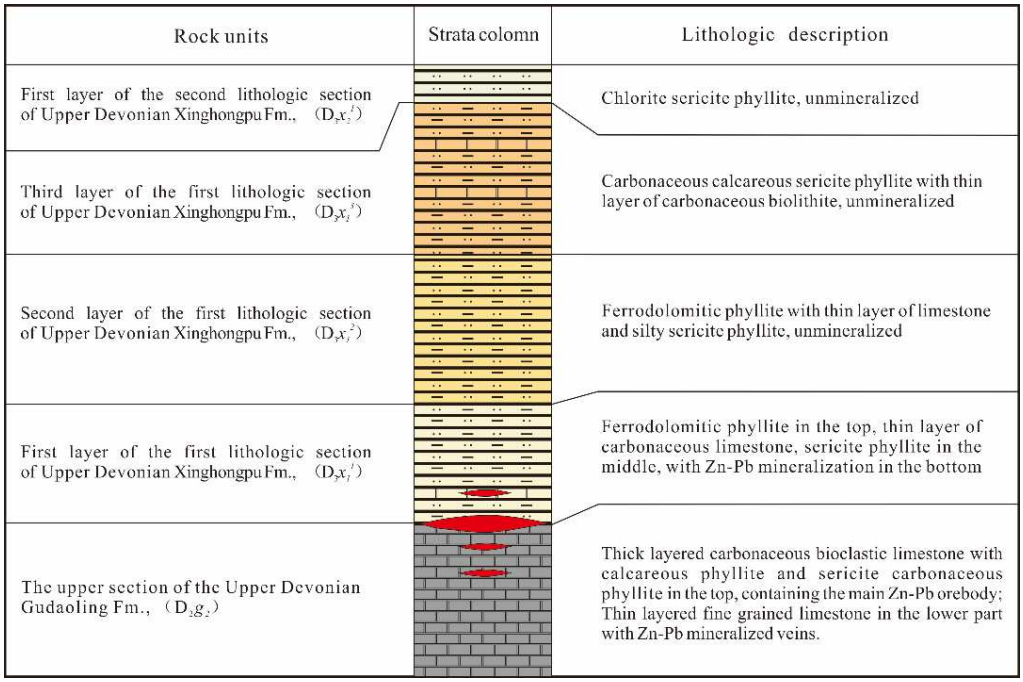

Figure 3. Stratigraphic column of the Dongtangzi Zn-Pb deposit.

No large scale of igneous rocks have been found in the mine area. However, the intrusive dikes are well developed. There are several diorite porphyry dikes and granite porphyry dikes, filling the NE-trending and NWW-trending faults, respectively. The former dikes crosscut the main orebody, while the latter dikes with zircon U-Pb ages of 226 ~ 221 Ma (LA-ICP-MS; Chen S.C. et al., 2020) are roughly parallel to the main orebody (Figure 3, Figure 4a). The main minerals of the granite porphyry dikes are plagioclase (30%), potash feldspar (35%), quartz (30%), biotite (3%), pyrite, zircon, sphene, etc (Figure 4b, c). The existance of cataclastic quartz suggests that the dike has underwent tectonic deformation after its emplacement (Figure 4b, c).

Preprints (www.preprints.org) | NOT PEER-REVIEWED | Posted: 11 January 2024 doi:10.20944/preprints202401.0877.v1

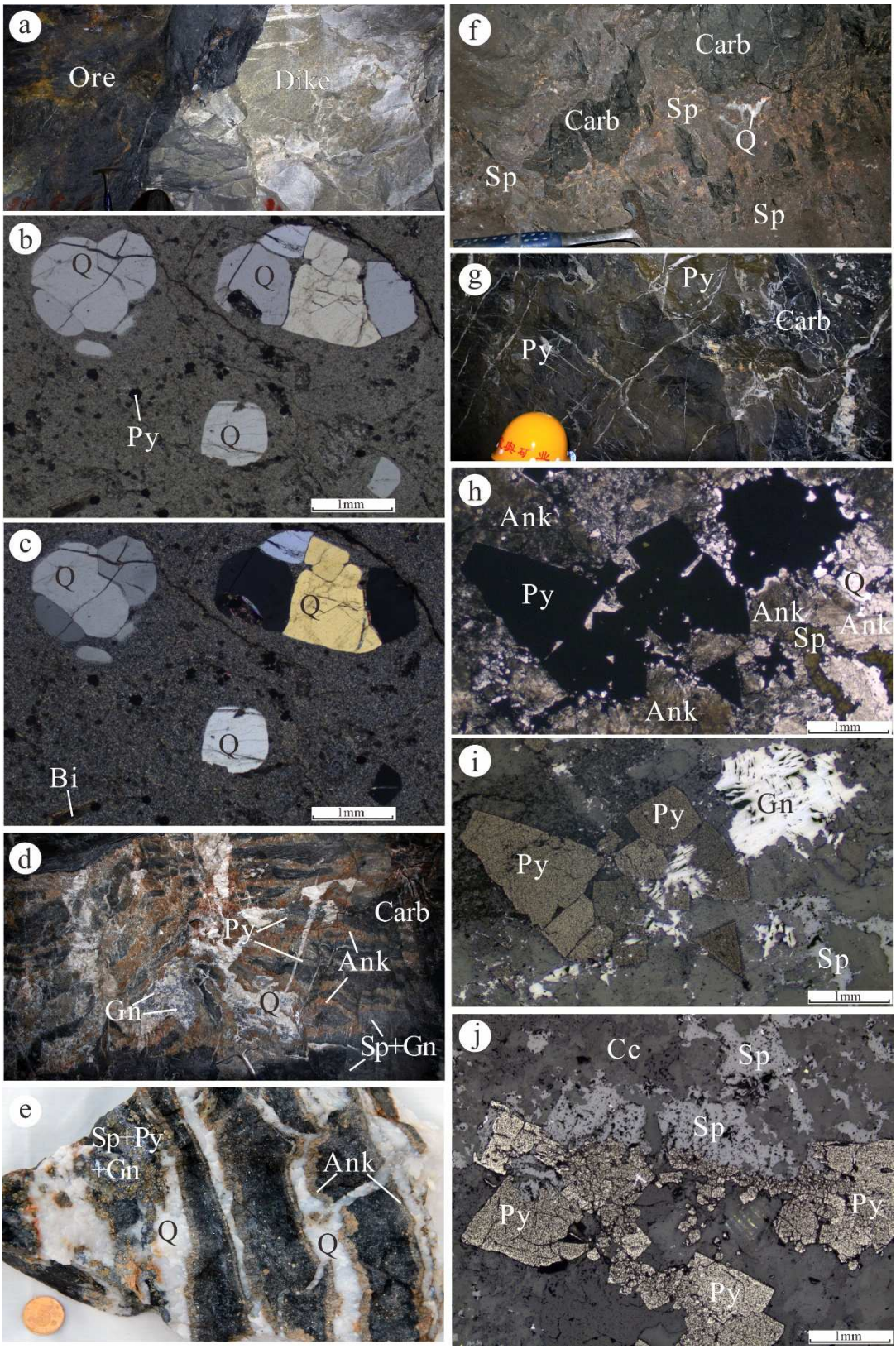

Figure 4. Rocks of the Dongtangzi Zn-Pb deposit. a. The NWW-trending granite porphyry dike crosscutting the main orebody. b, c. Subhedral granular quartz phenocrysts in the granite porphyry (b - plane-polarized light; c - cross-polarized light). d. Breccia type ore. The brecciated alterated carbonaceous limestone with disseminated sulfides inside and ankerite at the edges, cementing by medium - coarse-grained quartz + dolomite + polymetallic sulfide. e. Veinlet ore. Quartz + sulfide + ankerite veins crosscutting the brecciated alterated carbonaceous limestone. f. Sphalerite-rich massive

Preprints (www.preprints.org) | NOT PEER-REVIEWED | Posted: 11 January 2024 doi:10.20944/preprints202401.0877.v1

ore cementing the dolomitized alterated rocks. g. Pyrite-rich massive ore with metasomatic remnant alterated carbonates. h, i. The euhedral granular pyrite was metasomatized by sphalerite and galena within the pyrite-rich ore (h - plane-polarized light; i – reflected light). j. The fragmented pyrite metasomatized by sphalerite (reflected light). Abbreviations: Sp = sphalerite, Gn = galena, Py = pyrite, Q = quartz, Ank = ankerite, Cc = calcite, Carb = carbonate.

3.3. Orebodies

Controlled by the Qiandongshan-Dongtangzi anticline, the main orebody occurs at the contact zone between the Devonian Gudaoling Formation (D_2g) and the Xinghongpu Formation (D_3x) (Figure 2, 3), which is composed of the No.1 orebody (north subsidiary anticline) and the No.2 ore body (south subsidiary anticline), accounting for more than 90% of the total Zn-Pb reserves. The No.1 ore body extending 2.35 times its depth (Zeng L.G., 2009). The other ore bodies occur within the fault fracture zones and irregular tensile fractures in limestone, or within interlayer fractures in phyllite, with relatively small scale and unstable occurrence (Figure 2b, 3). The eastern part of the No.1 ore body occurs in the northern wing of the anticline and the saddle of the northern subsidiary anticline, and there is a trend of pinching out westward (Figure 2). The No. 2 ore body, located on the southern wing of the anticline, is larger in scale in the west part within the Dongtangzi mine section (Figure 2). The orebodies in the north wing of anticline are thiner and the wall rocks are strong foliated, while the orebodies in the south wing of anticline are thicker, with wall rocks not obviously foliated. In addition, within the carbonaceous limestone near the footwall of the No. 2 orebody, a cryptoexplosion breccia pipe was discovered, with different sizes of angular-sub angular breccias, composed of granite porphyry, quartz vein, altered rock, and massive sulfide ore, cemented with argillaceous and carbonaceous (Figure 5a).

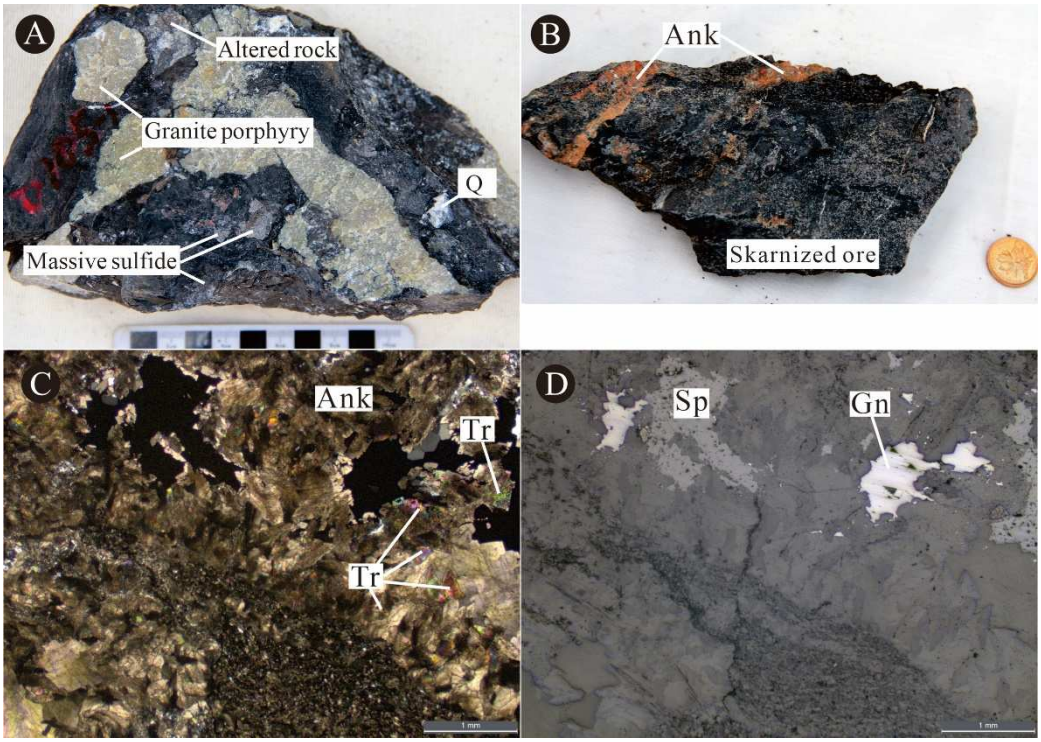

Figure 5. Cryptoexplosive breccia and skarn in the Dongtangzi Zn-Pb deposit. A. Cryptoexplosive breccias, with different sizes of angular-sub angular breccias, composed of altered granite porphyry, quartz aggregate, altered carbonaceous limestone, and massive sulfide ores, cemented by argillaceous and carbonaceous; B. Skarnized brecciated ore beside the granite porphyry dike; C, D. Microscopic image of the skarnized ore, ankerite replaced by tremolite, which occurs at the edge of fine-grained disseminated sphalerite and galena aggregate (C cross-polarized light, D reflected light). Note: Sp-sphalerite, Q-quartz, Gn-galena, Ank-ankerite, Tr-tremolite.

Preprints (www.preprints.org) | NOT PEER-REVIEWED | Posted: 11 January 2024 doi:10.20944/preprints202401.0877.v1

The ore minerals are mainly comprised of sphalerite, galena, pyrite, chalcopyrite, and arsenopyrite. The gangue minerals include quartz, ankerite, dolomite, calcite, siderite, sericite, chlorite, and apatite. The ore structures are mainly veinlets (Figure 4e), banded, brecciated (Figure 4d, f), blocky (Figure 4g), banded, and disseminated. Extensively vein filling and metasomatic mineralization can be observed in all the orebodies. The ore textures include granular (Figure 4h, i), metasomatic (Figure 4h, i, j), fragmented (Figure 4j), and wrinkling pressure shadow texture. The wall-rock alteration is widely and intensively developed throughout the floor and roof rocks, including silicification, dolomitization, calcitization, pyritization, sericitization, graphitization, etc. In addition, skarnization was developed in the ore beside the granite porphyry dikes (Figure 5b, c, d).

3.4. Mineralogy assemblage and paragenetic sequence

Based on systematic observation of mineral assemblages, ore structure and texture, hydrothermal alteration, and crosscutting relationships of multistage veins in the Dongtangzi Zn-Pb deposit, the paragenetic association can be divided into two periods, namely the sedimentary period and the hydrothermal mineralization period, respectively. The Hydrothermal mineralization period can be further divided into three stages (Figure 6): Stage I, a polymetallic sulfide – ankerite – quartz stage; Stage II, a quartz – pyrite-rich sulfide – ankerite stage; and stage III, a quartz – carbonate – sulfide stage.

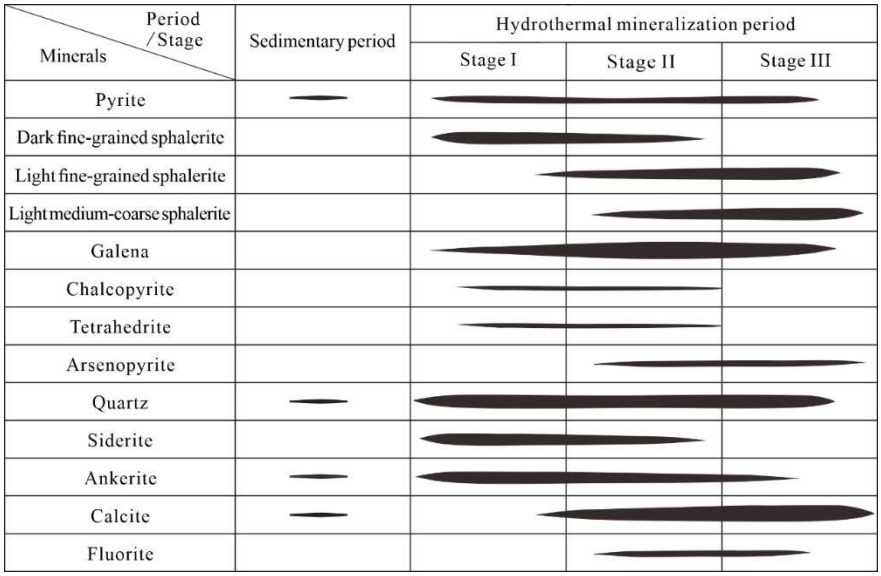

Figure 6. Mineral paragenetic sequence of the Dongtangzi Zn-Pb deposit.

3.4.1. Sedimentary period

There is no obvious Zn-Pb mineralization in the sedimentary period, and the syn-sedimentary pyrite (Py_0) are observed, which are mostly metasomatized by sulfides and quartz during the hydrothermal period (Figure 8a, b, c). No significant syn-sedimentary characteristics like clastic texture or laminated texture have been found in Pb-Zn ores, as the primary sedimentary textures were mostly destroyed by the structural deformation and metamorphism, syngenetic minerals are mostly replaced, deformed, and cemented by hydrothermal minerals during the hydrothermal mineralization period.

Preprints (www.preprints.org) | NOT PEER-REVIEWED | Posted: 11 January 2024 doi:10.20944/preprints202401.0877.v1

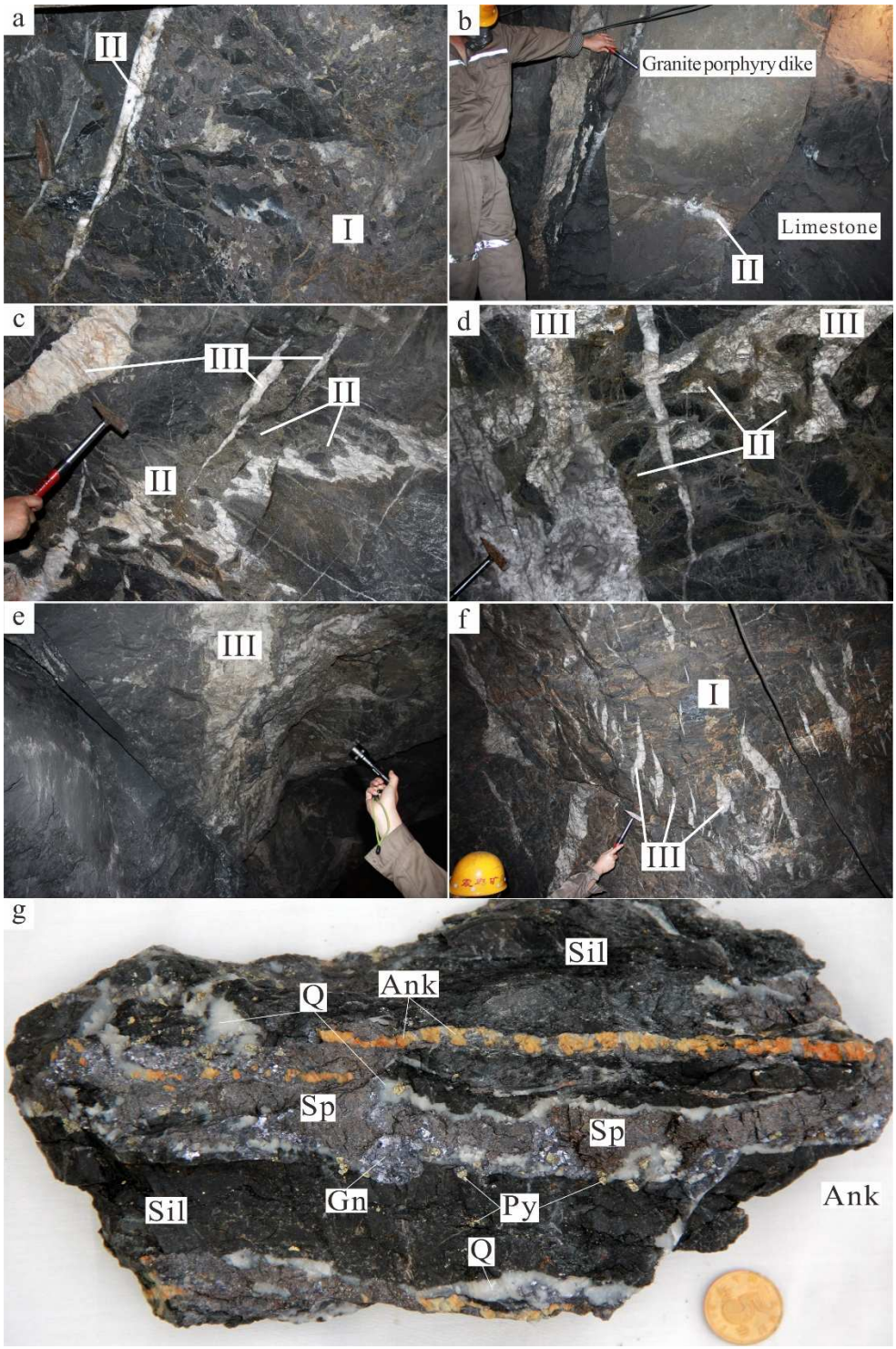

Figure 7. Occurrence features of the different mineralizaion stages in the Dongtangzi Zn-Pb deposit. a. The Stage I massive and brecciated ores intersected by the Stage II quartz – pyrite - ankerite veins; b. The granite porphyry dike is crosscut by the Stage II quartz – pyrite - sphalerite vein; c. The Stage II pyrite-rich ore is crosscut by Stage III quartz – calcite veins; d. The Stage II pyrite - ankerite vein is crosscut by the Stage III calcite veins; e. The Stage III coarse-grained calcite - pyrite vein; f. The Stage III quartz - pyrite - sphalerite veins are arranged in echelon, crosscutting the Stage I ores; g. The Stage I quartz - sphalerite - galena - pyrite - ankerite parallel veins crosscutting the carbonaceous alterated rocks. Note: Sp - sphalerite, Q - quartz, Gn - galena, Ank - ankerite, Sil - siliceous rock.

Preprints (www.preprints.org) | NOT PEER-REVIEWED | Posted: 11 January 2024 doi:10.20944/preprints202401.0877.v1

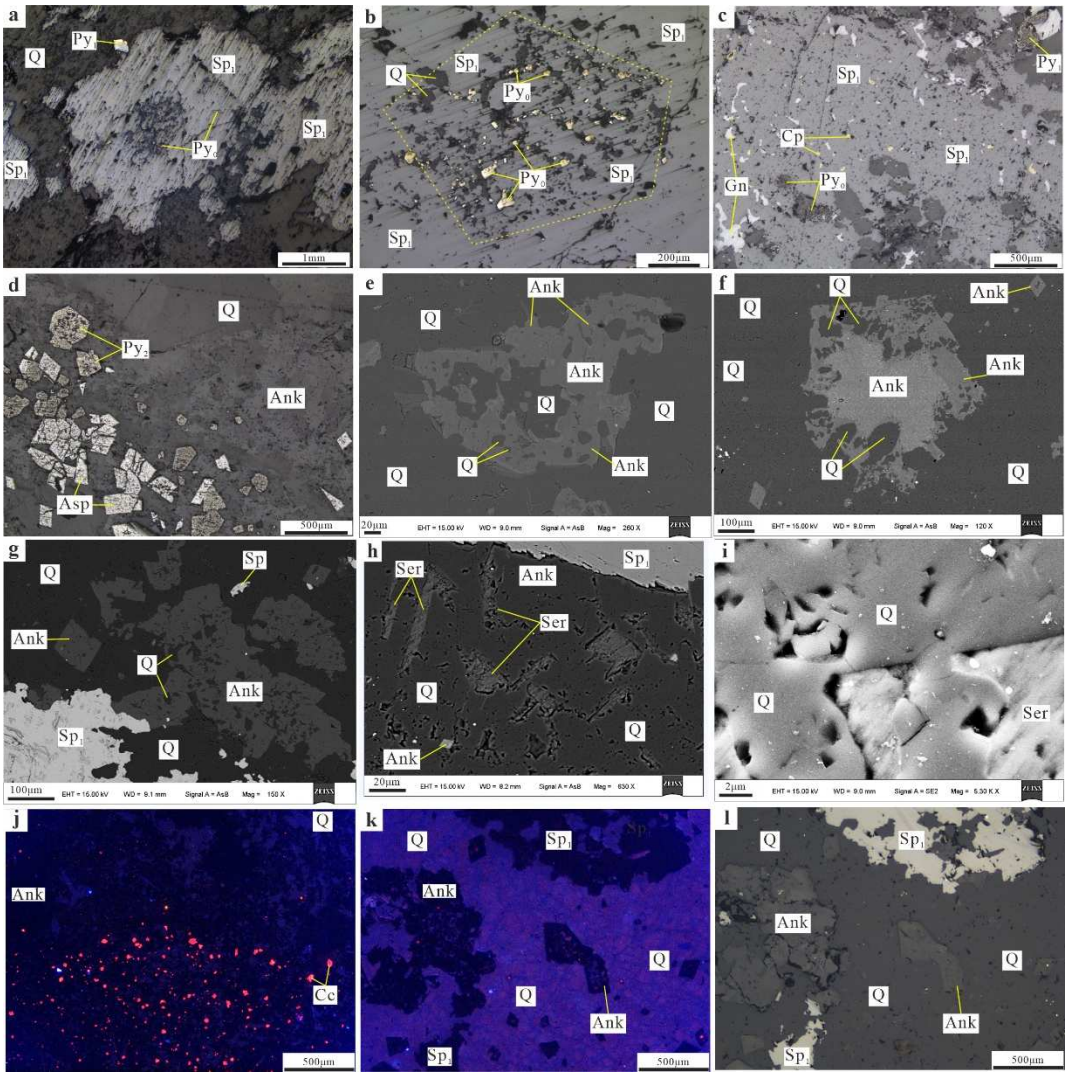

Figure 8. Microfabric characteristics of the ore in the Dongtangzi Zn-Pb deposit. a, b. Metasomatic residual skeleton texture of the pyrite (Py_0) replaced by the sphalerite (Sp_1), under reflected light; c. Droplet chalcopyrite, irregular galena and metasomatic residual Py_0 are developed in the massive sphalerite (Sp_1), under reflected light. d. Densely disseminated pyrite (Py_2) + arsenopyrite (Asp_2) developed in the ferrodolomite siliceous rock, under reflected light; e, f. The ankerite in the siliceous rock is replaced by quartz, forming skeletal crystal texture, BSE image; g. Ankerite in the siliceous rocks are metasomatized by quartz and sphalerite; h. Microfine quartz, sericite and ankerite together in the siliceous rocks, with sphalerite filling in cracks; i. Scanning electron microscopy (SEM) images show that the surface of the quartz developed triangular pores, with tightly cemented grains, flat edges, and crystal textures. j. Cathode luminescence (CL) image of the ankerite siliceous rock. The residual of metasomatized calcite is orange colored, while the ankerite is black, and the quartz is deep bluish purple; k, l. the silicate rocks are metasomatized by quartz and sphalerite (k - cathode luminescence, l - reflected light).

3.4.2. Hydrothermal mineralization period

Stage I: A polymetallic sulfide – ankerite - quartz stage

The stage I is rich in sphalerite and galena, with pyrite locally enriched, accompanied with less chalcopyrite. The sphalerite is fine-grained, mainly dark brown in color. The galena and pyrite are fine-grained - aphanitic, cementing the breccia of the carbonaceous altered rock (Figure 7a). The stage I ore developed silicification, dolomitization, chloritization, and locally sericitization, replacing the banded marl along bedding, or filling the tension fractures within the carbonaceous limestone (Figure 7g). Carbonates are extensively metasomatized by quartz and sulfides (Figure 8e, f, g), and some

Preprints (www.preprints.org) | NOT PEER-REVIEWED | Posted: 11 January 2024 doi:10.20944/preprints202401.0877.v1

quartz and sulfides retain the skeleton crystal structure of carbonates (Figure 8e, f). The stage I is the main mineralization stage, which is generally affected by later tectonic deformation, developing fragmentation and locally recrystallization (Figure 4d, 7a, 7f).

No obvious sedimentary mineralization characteristics has been found in the ore of the Dongtangzi Zn-Pb deposit. For example, (1) the sheet-like sericite among quartz grains is irregularly (Figure 8h), without obvious orientation, and does not have typical sedimentary texture of directional arrangement of argillaceous minerals; (2) Quartz grains are crystalline and tightly cemented between grains (Figure 8i), with no obvious grinding round texture, showing no syn-sedimentary characteristics, indicating that the quartz in the altered rocks could be brought by the hydrothermal fluid running through the fracture systems of different scales; (3) Most of the quartz in the altered rocks are obviously formed by metasomatism, as the calcite (orange region in Figure 8j) is replaced by ankerite (black region in Figure 8j) and quartz (blue-purple region in Figure 8j), while the ankerite (Figure 8k, l) is replaced by quartz (blue-purple region in Figure 8k) and sphalerite (Figure 8k, l), indicating that the altered rocks were formed by remarkably silicification and replacement of carbonate rocks by siliceous hydrothermal fluid, rather than by sedimentary exhalative processes suggested by some researchers (Lu and Wei, 1992; Qi et al., 1993; Fang W.X., 1997, 1999b).

Stage II: A quartz - pyrite-rich sulfide – ankerite stage

The stage II quartz - pyrite - ankerite - veins are accompanied by polymetallic sulfides such as sphalerite, galena, chalcopyrite and arsenopyrite, which are generally coarse-grained. The Zn-Pb mineralization scale of this stage is smaller than the stage I, but is more enriched in pyrite, locally intersecting and replacing the stage I ore and wall rock (Figure 7a), meanwhile crosscutting the granite porphyry dikes (Figure 7b), with scattered pyritization within the granite porphyry dike on both besides of the stage II quartz vein. According to the interspersion relationship, the NWW-trending granite porphyry dike locally crosscuts the Stage I orebody, and is cut through by the quartz-sulfide vein of the Stage II, indicating that it was emplaced at a time between stage I and stage II. The sphalerite is medium-fine grained, mainly light brown in color. No apparent replacement was observed on the pyrite (Py_2) and arsenopyrite (Asp_2) in the altered rocks (Figure 8d). Dolomitization, pyritization, and silicification are well developed in the wall rocks during the stage II (Figure 7c, d).

Stage III: A quartz – carbonate – sulfide stage

The Stage III quartz – carbonate – sulfide veins are widely developed in the whole deposit, forming NE-trending joint veins or en echelon veins (Figure 7f). It mainly consists of coarse-grained quartz and calcite (Figure 7e), with coarse– medium-grained ankerite, pyrite, galena, and sphalerite. The extension range of the veins is small, crosscutting the wall rocks and the ore veins of the first two stages (Figure 7c, d). The wall rock alteration is weak, including silicification, pyritization, carbonation.

4. Samples and analytical methods

All samples utilized in this work were collected from underground tunnels at diverse depths within the Dongtangzi Zn-Pb deposit. After making the polished thin sections, comprehensive microscopic observation was carried out to preliminarily characterize the morphology, textures and paragenesis of ore-related minerals. Subsequently, representative samples were chosen for further analyses (Table 1). A subset of these samples underwent crushing, with sulfide minerals, including sphalerite, galena, and pyrite, meticulously hand-picked under a binocular microscope. The purity of individual mineral separations exceeded 99%, and all mineral isolations underwent thorough cleaning in an ultrasonic bath. Concurrently, other portions of the samples were polished into thin sections, facilitating high-precision in-situ LA-MC-ICP-MS sulfur and lead isotope analyses.

Table 1. Samples description of the Dongtangzi Zn-Pb deposit.

No.	Sample	Position	Stage	Type	Description
1	D216.3-1	960 m elevation, north south of the No.2 ore body	I	Siliceous rock	Siliceous rock with pyrite of the sedimentary

Preprints (www.preprints.org) | NOT PEER-REVIEWED | Posted: 11 January 2024 doi:10.20944/preprints202401.0877.v1

					mineralization period, intersected by the hydrothermal Stage I quartz-pyrite-galena veins
2	D22	1010 m elevation, south wing of the No.2 ore body	I	Disseminated ore	Lamellar carbonaceous altered rock, with disseminated medium-fine grained sphalerite
3	D28-4	960 m elevation, south wing of the No.2 ore body	I	Banded ore	Fine-grained quartz-ankerite-pyrite veins are zebra striated in carbonaceous altered rocks
4	D29-1	960 m elevation, south wing of the No.2 ore body	I	Vein type ore	Quartz-dolomite-sphalerite-pyrite-galena veins developed in carbonaceous limestone
5	D45	960 m elevation, south wing of the No.2 ore body	I	Massive, brecciated ore	Medium-coarse grained massive sphalerite- pyrite-dolomite aggregate, locally cementing breccias of carbonaceous altered rock
6	D48	860 m elevation, saddle part of the No.2 ore body	I	Disseminated ore	Fine-grained sphalerite, galena, pyrite and dolomite are densely disseminated in altered rocks
7	DTZ-2-2	1060 m elevation, saddle part of the No.2 ore body	I	Mineralized carbonaceous limestone	Quartz-calcite veins are interspersed with carbonaceous limestone, with black aphanitic sphalerite developed at the edges
8	DTZ-1	1060 m elevation, south wing of the No.2 ore body	I	Mineralized carbonaceous phyllite	The carbonaceous phyllite contains lumpy, disseminated sphalerite, galena and pyrite
9	DTZ-3-4	1060 m elevation, north wing of the No.2 ore body	I	Massive ore	Fine-grained black brown lumpy sphalerite, with less quartz, pyrite and galena
10	D41	860 m elevation, south wing of the No.2 ore body	I	Disseminated ore	Fine-grained sphalerite and ankerite are densely disseminated in grayish-black carbonaceous altered rocks
11	D213.2	960 m elevation, north wing of the No.2 ore body	I	Mineralized siliceous rock	Gray - black siliceous rock with disseminated fine - grained pyrite

Preprints (www.preprints.org) | NOT PEER-REVIEWED | Posted: 11 January 2024 doi:10.20944/preprints202401.0877.v1

12	D51-1	795 m elevation, south wing of the No.2 ore body	I	Disseminated ore	Fine-grained sphalerite, galena, pyrite and dolomite are densely disseminated in altered rocks
13	D61-1	910 m elevation, saddle part of the No.2 ore body	I	Disseminated ore	Medium - fine - grained dense disseminated sphalerite, pyrite and arsenopyrite are developed in silicified carbonaceous limestone
14	D229-1	960 m elevation, south wing of the No.2 ore body	I	Banded ore	Banded ankerite-sphalerite-pyrite-galena veins developed in altered carbonaceous limestone
15	D36	910 m elevation, south wing of the No.2 ore body		Granite porphyry dike	NWW-trending granite porphyry dike, nearly parallel to the ore body, with scattered pyrite
16	D55	960 m elevation, south wing of the No.1 ore body	II	Disseminated ore	Quartz-dolomite stockwork developed in the limestone, with fine-grained arsenopyrite and pyrite aggregate developed at the contact area
17	D58	960 m elevation, south wing of the No.1 ore body	II	Disseminated ore	Silicified limestone with disseminated pyrite, interspersed by quartz-dolomite stockwork
18	D107-3	795 m elevation, south wing of the No.2 ore body	II	Massive ore	The massive medium-fine grained pyrite-sphalerite-arsenopyrite-ankerite aggregates, interspersed by the Stage III coarse-grained calcite and galena veins
19	D109	795 m elevation, south wing of the No.2 ore body	II	Massive ore	Pyrite-rich massive ore, micro-fine grained pyrite aggregates, cementing carbonaceous altered breccia
20	D205.2	795 m elevation, south wing of the No.2 ore body	II	Vein type ore	Veinlets composed of quartz, calcite, pyrite, sphalerite, and galena, crosscutting the altered rocks

Preprints (www.preprints.org) | NOT PEER-REVIEWED | Posted: 11 January 2024 doi:10.20944/preprints202401.0877.v1

21	D26	960 m elevation, saddle part of the No.2 ore body	III	Vein type ore	The medium-fine grained lumpy sphalerite, galena and calcite vein developed in the altered carbonatite
22	D230	960 m elevation, south wing of the No.2 ore body	III	Disseminated ore	Veinlet-disseminated ore, mineralized siliceous rock crosscutting by quartz-calcite-pyrite veins
23	D37-2	910 m elevation, north wing of the No.1 ore body	III	Gold bearing ore	The altered marl, with disseminated pyrite, interspersed with quartz-dolomite-pyrite vein
24	D223.3	795 m elevation, south wing of the No.2 ore body	III	Gold bearing ore	Dense disseminated pyrite is developed in the altered rock, with quartz-calcite aggregates

4.1. In-situ S isotope analysis

Representative sphalerite, pyrite, and galena crystals of hydrothermal stage I to stage III, pyrite of sedimentary period, and pyrite of granite porphyry dike were selected for in-situ LA-MC-ICP-MS sulfur isotope analysis by using a Resonetics-S155 excimer ArF laser ablation system with Nu Plasma II multicollector ICP-MS at the State Key Laboratory of Geological Processes and Mineral Resources, China University of Geosciences, Wuhan. Detailed test methods follow Fu et al. (2016) and Zhu et al. (2016, 2017). The energy fluence of the laser is approximately 3 J/cm^2. For single spot analysis, the diameter is 33 μm with a laser repletion rate of 8 Hz. The true sulfur isotope ratio was calculated by correction for instrumental mass bias by linear interpolation between the biases calculated from two neighboring standard analyses. Isotope data are reported in delta notation (‰) in comparison with Vienna Cañon Diablo Troilite (V-CDT):

$$\delta^{34}S_{V\text{-}CDT} = [((^{34}S/^{32}S)_{sample}/ (^{34}S/^{32}S)_{V\text{-}CDT}) -1] \times 10^3$$

Where $(^{34}S/^{32}S)$ sample is the measured $^{34}S/^{32}S$ ratio in the sample and $(^{34}S/^{32}S)_{V\text{-}CDT}$ is defined as 0.044163 (Ding et al., 2001). The precision of $^{34}S/^{32}S$ analysis is less than 0.00003 (1δ). An in-house pyrite standard named WS-1 was used to calibrate the mass bias for S isotopes (Zhu et al., 2016). This consists of a natural pyrite crystal from the Wenshan polymetallic skarn deposit, Yunnan Province, China. The $^{34}S_{V\text{-}CDT}$ value (0.3 ± 0.1%) for WS-1 natural pyrite was determined using the CF-IRMS method on a MAT 253 isotope ratio mass spectrometer (Thermo Finnigan, Bremen, Germany) at the Institute of Mineral Resources, Chinese Academy of Geological Sciences, Beijing. Standards were measured before, and after every four spot analyses. We also use the pyrite standard to get data of galena and sphalerite, and these data should be considered as roughly results due to no proper standard.

4.2. In-situ Pb isotope analysis

26 analysis spots, including pyrite, galena and sphalerite of hydrothermal stages I~III and pyrite of the granite porphyry dike, were selected for in-situ LA-MC-ICP-MS lead isotope analysis. The examination was conducted utilizing a 193 nm laser ablation system (RESOlution M-50, ASI) interfaced with a Nu Plasma II multicollector ICP-MS (Wrexham, UK) at the State Key Laboratory of Continental Dynamics, Department of Geology, Northwest University, Xi'an. Homogeneous nano-particulate pressed sulfide powder tablets (PSPTs) served as reference materials to ensure

Preprints (www.preprints.org) | NOT PEER-REVIEWED | Posted: 11 January 2024 doi:10.20944/preprints202401.0877.v1

measurement accuracy. Instrument parameters were optimized using the NIST610 standard (Pb=426 μg/g) to achieve maximal analytical sensitivity, signal stability, and optimal peak shape and alignment. Analytical signals were deduced using the Time Resolved Analysis (TRA) mode, with an integration time of 0.2 s. Each measurement spot encompassed a 30 s background measurement, followed by 50 s of ablation for signal collection, and an additional 120 s for wash time to mitigate memory effects. Galena laser ablation operated at a frequency of 2 Hz with a spot size of 9 μm, while for bismuthinite, the frequency was 6 Hz with a spot size of 30 μm, respectively. The ^{202}Hg, ^{203}Tl, ^{204}Hg+^{204}Pb, ^{205}Tl, ^{206}Pb, ^{207}Pb, and ^{208}Pb ion beams were collected by corresponding Faraday cups. The ^{204}Hg/^{202}Hg natural abundance ratio (0.229883) was used to calculate and determine the interference from the ^{204}Hg species on the ^{204}Pb intensity obtained. Analytical procedures, reference material PSPTs, and data processing has been previously described in detail by Chen et al. (2014), Yuan et al. (2015), and Bao et al. (2017).

4.3. Rb–Sr isotope analyses

The sulfide samples of the Stage I were rinsed several times in distilled water, dried, and crushed to 40–60-mesh size. The individual minerals of sphalerite and pyrite were handpicked under a binocular microscope, with purity levels of >98% being used for analysis. Sulfide grains were crushed to <200 mesh using an agate ball mill, then washed in an ultrasonic bath and dried. For Rb−Sr isotope analyses, powder weighing 0.2–0.3 g of each sample were dissolved in Teflon beakers with a mix of HF and HNO_3 acids. Rb−Sr have been separated for isotopic analysis by adopting resin of AG50W×8 and different eluent reagents. Firstly, REEs are separated from Rb−Sr by using normal method of cation−exchange chromatography with eluent of HCl. Then Rb and Sr were separated using cation ion exchange column.

Sulfide samples underwent Rb–Sr isotopic analyses using a VG 354 mass spectrometer equipped with five collectors at the Center of Modern Analysis, Nanjing University. The chemical separation and mass spectrometric procedures are outlined by Wang et al. (2006). ^{87}Sr/^{86}Sr is normalized to ^{86}Sr/^{88}Sr = 0.1194, to correct for instrumental fractionation. During the period of this study, measurements for the American Standard Reference Material NBS 987 Sr standard gave ^{87}Sr/^{86}Sr = 0.710236 ± 0.000007 (2σ).

4.4. Sm-Nd isotope analyses

The carbonate minerals of ankerite, dolomite and calcite in the Dongtangzi Zn-Pb deposit were systematically collected from hydrothermal mineralization period sphalerite–galena–pyrite–quartz–ankerite–dolomite–calcite veins within the main orebody, with 6 samples of the Stage I, 2 of the Stage II, and 1 of the Stage III, respectively (Table 5). These carbonate minerals were separated from the ore samples after crushing and were powdered in an agate mill before Sm–Nd isotopic analysis.

Powders of carbonate mineral specimens underwent dissolution utilizing purified 0.5 M dilute acetic acid at ambient temperature over a four-hour duration. After centrifugation, acid-insoluble residues underwent digestion employing a mixture of HNO_3, HF, and $HClO_4$, rendering them amenable for Nd isotopic analyses. The Nd solutions were subjected to separation through conventional ion exchange techniques. The isotopic compositions of the refined Nd solutions were quantified utilizing a VG 354 mass spectrometer equipped with five collectors at the Center of Modern Analysis, Nanjing University. A comprehensive account of the experimental methodology can be found in the reports by Wang Y.X. et al. (2007) and Li et al. (2007).

5. Results

5.1. In-situ S isotopic compositions

A total of 50 spots were performed for in-situ sulfur isotope study covering the pyrite of sedimentary period (n=4), the sulfides of the hydrothermal period stage I (n=23), stage II (n=4), stage III (n=7), and the pyrite in the granite porphyry dike (n=4). The results are listed in Table 2 and shown in Figure 11b.

Preprints (www.preprints.org) | NOT PEER-REVIEWED | Posted: 11 January 2024 doi:10.20944/preprints202401.0877.v1

Table 2. In-situ S isotopic composition of the sulfides from the Dongtangzi Zn-Pb deposit.

Sample/Point No.	Stage	Mineral	$\delta^{34}S$ (‰)
D216.3/1	Sedimentary period	Pyrite	16.9
D216.3/2		Pyrite	15.8
D216.3/5		Pyrite	19.9
D216.3/6		Pyrite	21.4
D216.3/3	Hydrothermal I	Sphalerite	7.3
D216.3/4		Sphalerite	8.7
D41/1		Sphalerite	9.1
D41/2		Pyrite	8.6
D41/3		Sphalerite	9.3
D41/4		Sphalerite	9.4
D41/5		Sphalerite	8.8
D51/1		Pyrite	8
D51/2		Galena	2.7
D51/3		Sphalerite	7.3
D51/4		Sphalerite	7
D51/5		Sphalerite	8
D51/6		Galena	1.4
D51/7		Galena	2.7
D51/8		Pyrite	7.1
D51/9		Sphalerite	7.1
D61/1		Pyrite	5.3
D61/2		Sphalerite	8.6
D61/3		Galena	1.1
D61/4		Sphalerite	8.8
D61/5		Sphalerite	8.9
D213.2/1		Sphalerite	8.3
D213.2/2		Sphalerite	8.8
D36.1/1	Granite porphyry dike	Pyrite	2.1
D36.1/2		Pyrite	4.3
D36.1/3		Pyrite	3.7
D36.1/4		Pyrite	2.5
D205.2/1	Hydrothermal II	Pyrite	7.4
D205.2/2		Chalcopyrite	6.4
D205.2/3		Pyrite	7.3
D205.2/4		Chalcopyrite	6.5
D26/1	Hydrothermal III	Sphalerite	9.9
D26/2		Galena	4.4
D26/3		Sphalerite	9.5

Preprints (www.preprints.org) | NOT PEER-REVIEWED | Posted: 11 January 2024 doi:10.20944/preprints202401.0877.v1

D26/4	Galena	4.8
D26/5	Sphalerite	9.9
D26/6	Pyrite	10.2
D26/7	Sphalerite	9.3
D26/8	Galena	4.6
D223.3/1	Pyrite	8.9
D223.3/2	Pyrite	3.8
D223.3/3	Pyrite	5
D223.3/4	Pyrite	4.4
D223.3/5	Pyrite	8.7
D223.3/6	Pyrite	7.2
D223.3/7	Pyrite	8.3

Preprints (www.preprints.org) | NOT PEER-REVIEWED | Posted: 11 January 2024 doi:10.20944/preprints202401.0877.v1

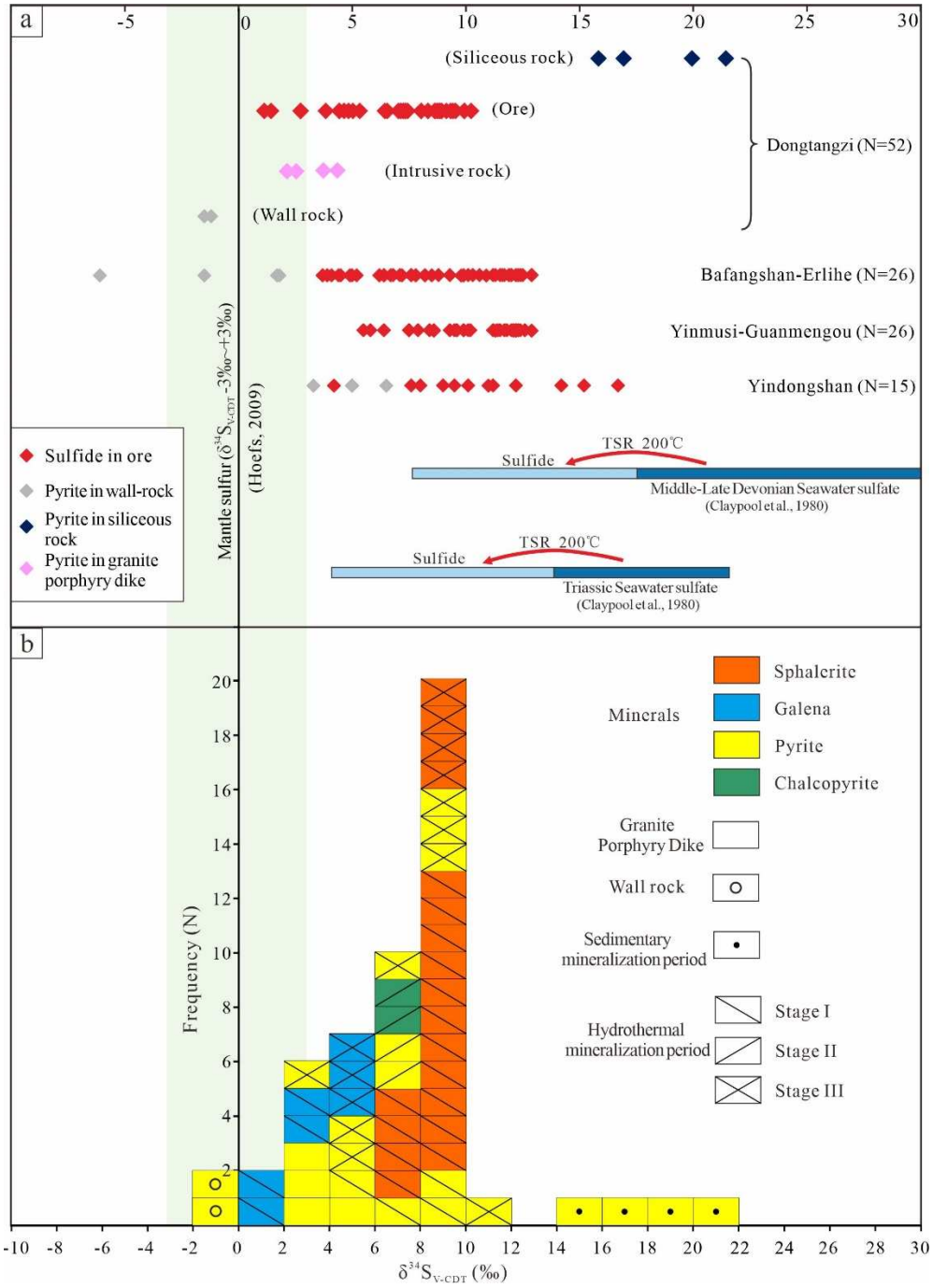

Figure 11. (a) Comparison diagram of sulfur isotope of the Pb-Zn deposits in the Fengtai ore cluster and (b) sulfur isotopic composition histogram of sulfides of the Dongtangzi Zn-Pb deposit. Note: The data of pyrite in the wall rock of the Dongtangzi deposit (gray dots) are from Wang J.L. et al. (1996), and the others are obtained from this work. The data of the Bafangshan-Erlihe, Yinmusi-Guanmengou and Yindongshan deposits are from Hu Q.Q. (2015), and the data of the middle - late Devonian and Triassic Marine sulfate are from Claypool et al. (1980).

The measured $\delta^{34}S$ data of the pyrite of the sedimentary period and the granite porphyry dike vary from 15.8 to 21.4‰ (averaging 18.5‰), and from 2.1 to 4.3‰ (averaging 3.2‰), respectively. While those of the sulfides from the three hydrothermal mineralization stages vary from 1.1 to 9.4‰ (averaging 7.1‰), from 6.4 to 7.4‰ (averaging 6.9‰), from 3.8 to 10.2‰ (averaging 7.3‰), respectively, showing a relatively restricted range, indicating that the source of sulfur has no significant difference during the hydrothermal mineralization period.

Preprints (www.preprints.org) | NOT PEER-REVIEWED | Posted: 11 January 2024 doi:10.20944/preprints202401.0877.v1

5.2. In-situ Pb isotopic compositions

All the sulfides analyzed have similar lead isotope values and the radioactive lead content are low (Table 3). The $^{206}Pb/^{204}Pb$, $^{207}Pb/^{204}Pb$ and $^{208}Pb/^{204}Pb$ ratios of the Stage I are 18.074-18.107, 15.641-15.663 and 38.217-38.764, respectively. And those of the Stage II are 18.073-18.082, 15.652-15.659 and 38.301-38.324, respectively. For the Stage III, the ratios are 18.078-18.265, 15.645-15.654 and 38.293-38.310, respectively. While for the granite porphyry dike, the ratios are 18.091-18.101, 15.585-15.610 and 38.169-38.241, respectively.

Table 3. In-situ Pb isotopic composition of the sulfides from the Dongtangzi Zn-Pb deposit.

Sample/Point No.	Stage	Mineral	$^{208}Pb/^{204}Pb$	$^{207}Pb/^{204}Pb$	$^{206}Pb/^{204}Pb$
D36/1	Granite porphyry dike	Pyrite	38.189 ± 0.010	15.595 ± 0.004	18.091 ± 0.011
D36/2		Pyrite	38.241 ± 0.009	15.61 ± 0.004	18.101 ± 0.003
D36/3		Pyrite	38.169 ± 0.005	15.585 ± 0.002	18.092 ± 0.002
D51/2	Hydrothermal I	Pyrite	38.448 ± 0.005	15.663 ± 0.002	18.076 ± 0.003
D51/3		Pyrite	38.286 ± 0.004	15.652 ± 0.001	18.078 ± 0.002
D51/4		Pyrite	38.324 ± 0.004	15.65 ± 0.002	18.074 ± 0.002
D51/1		Sphalerite	38.764 ± 0.026	15.662 ± 0.005	18.075 ± 0.001
D51/1		Galena	38.336 ± 0.008	15.661 ± 0.003	18.084 ± 0.001
D51/2		Galena	38.319 ± 0.007	15.654 ± 0.003	18.105 ± 0.002
D51/3		Galena	38.234 ± 0.006	15.647 ± 0.002	18.096 ± 0.002
D51/4		Galena	38.234 ± 0.009	15.646 ± 0.003	18.086 ± 0.002
D61/1		Galena	38.217 ± 0.004	15.643 ± 0.002	18.107 ± 0.005
D61/2		Galena	38.222 ± 0.007	15.642 ± 0.002	18.102 ± 0.003
D61/3		Galena	38.218 ± 0.005	15.641 ± 0.002	18.096 ± 0.002
D61/4		Galena	38.293 ± 0.001	15.647 ± 0.001	18.087 ± 0.002
D61/5		Galena	38.291 ± 0.004	15.645 ± 0.001	18.090 ± 0.003
D205-2/1	Hydrothermal II	Pyrite	38.307 ± 0.024	15.652 ± 0.009	18.074 ± 0.002
D205-2/2		Pyrite	38.324 ± 0.006	15.659 ± 0.002	18.074 ± 0.002
D205-2/3		Pyrite	38.314 ± 0.005	15.655 ± 0.002	18.073 ± 0.002
D205-2/4		Pyrite	38.321 ± 0.005	15.659 ± 0.002	18.082 ± 0.001
D205-2/5		Pyrite	38.301 ± 0.007	15.65 ± 0.003	18.080 ± 0.001
D26/1	Hydrothermal III	Galena	38.301 ± 0.007	15.646 ± 0.003	18.097 ± 0.002
D26/2		Galena	38.306 ± 0.005	15.649 ± 0.024	18.086 ± 0.003
D26/3		Galena	38.299 ± 0.006	15.646 ± 0.002	18.091 ± 0.004
D26/4		Galena	38.293 ± 0.003	15.645 ± 0.001	18.265 ± 0.005
D26/5		Galena	38.310 ± 0.003	15.654 ± 0.001	18.078 ± 0.002

5.3. Rb-Sr isochron age

The analytical data are listed in Table 4. The Rb contents of the samples are low, ranging from 0.235×10^{-6} to 1.207×10^{-6}, and the Sr contents are also low, ranging from 0.3105×10^{-6} to 5.218×10^{-6}. The value of $^{87}Rb/^{86}Sr$ range from 0.528 to 6.971. The value of $^{87}Sr/^{86}Sr$ has a wide range from 0.71204

Preprints (www.preprints.org) | NOT PEER-REVIEWED | Posted: 11 January 2024 doi:10.20944/preprints202401.0877.v1

to 0.73148. Regression and age calculations of isochrons were performed using Isoplot/Ex Version 3.00 software (Ludwig, 2008), and with $\lambda = 1.42 \times 10^{-11} a^{-1}$, using 1% errors for $^{87}Rb/^{86}Sr$ ratios and 0.05% errors for $^{87}Sr/^{86}Sr$ ratios at a confidence level of 95%. The analytical data yielded an isochron age of 211.6 ± 2.6 Ma with an initial $^{87}Sr/^{86}Sr$ ratio of 0.71046 ± 0.00012 and MSWD value of 0.31 (Figure 9a).

Table 4. Analytical data of Rb–Sr isotope ratios and Rb–Sr contents.

Sample No.	Mineral	Stage	Rb (μg/g)	Sr (μg/g)	$^{87}Rb/^{86}Sr$	$^{87}Sr/^{86}Sr$	2σ
DTZ-2-2	Spalerite	I	0.4932	2.7590	0.5278	0.712041	0.000008
DTZ-1	Pyrite	I	1.2070	5.2180	0.6794	0.712506	0.000008
DTZ-1	Galena	I	0.2347	0.3742	1.8150	0.715902	0.000009
DTZ-1	Spalerite	I	0.7834	1.6930	1.3620	0.714581	0.000010
DTZ-3-4	Galena	I	0.3728	0.3105	3.5470	0.721159	0.000008
DTZ-3-4	Spalerite	I	0.9346	0.3957	6.9710	0.731475	0.000009

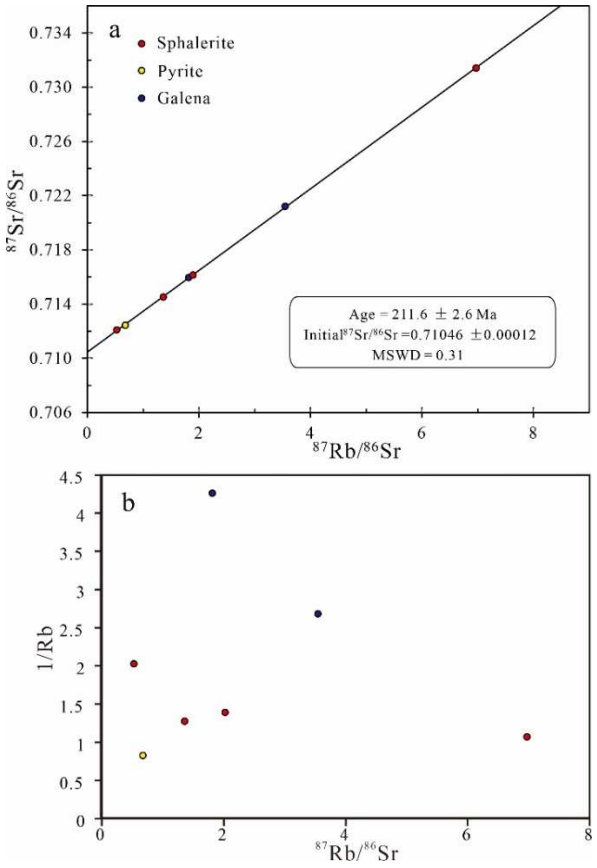

Figure 9. (a) Rb–Sr isochron age of sulfides from the Dongtangzi Zn-Pb deposit; (b) Diagram of 1/Rb versus $^{87}Rb/^{86}Sr$.

Considering the potential for physical deformation of the ore, there exists a plausible scenario where the determined ages might be influenced by tectonic overprint, necessitating further investigation of this aspect. The assessment of 1/Rb versus $^{87}Rb/^{86}Sr$ diagrams provides a way to discern whether the initial $(^{87}Sr/^{86}Sr)_i$ values remained constant throughout the sulfide growth process (Li et al., 2002), thereby enabling an evaluation of data integrity. In the present investigation, the absence of covariation between 1/Rb values and $^{87}Rb/^{86}Sr$ (Figure 9b) signifies that the isochron age data are meaningful, offering a reliable age of the ore formation.

5.4. Sm-Nd isochron age

Preprints (www.preprints.org) | NOT PEER-REVIEWED | Posted: 11 January 2024 doi:10.20944/preprints202401.0877.v1

All $^{143}Nd/^{144}Nd$ ratios determined for the samples of the hydrothermal mineralization period ankerite, dolomite and calcite analyzed during this study were normalized to $^{146}Nd/^{144}Nd = 0.7219$, with results and analytical uncertainties (2σ) given in Table 5. The $^{147}Sm/^{144}Nd$ values for carbonate minerals from stage I range from 0.0731 to 0.7195, with corresponding $^{143}Nd/^{144}Nd$ values range from 0.511851 and 0.512739.

Table 5. The Sm-Nd isotopic data of the stage I carbonates from the Dongtangzi Zn-Pb deposit.

Sample No.	Mineral	Stage	Sm($\times10^{-6}$)	Nd($\times10^{-6}$)	$^{147}Sm/^{144}Nd$	$^{143}Nd/^{144}Nd$
D22	Dolomite	I	0.1605	3.527	0.1351	0.511943±9
D28-4	Ankerite	I	0.6537	2.678	0.7195	0.512739±7
D29-1	Dolomite	I	0.4058	4.634	0.2586	0.512081±8
D45-31	Dolomite	I	0.1325	5.336	0.0731	0.511851±8
D45-32	Dolomite	I	0.3536	5.781	0.1803	0.511982±7
D48	Dolomite	I	0.2953	4.013	0.2175	0.512024±9
D55	Dolomite	II	0.4831	3.907	0.3656	0.512229±14
D58	Calcite	II	0.5029	2.694	0.5498	0.512501±8
D58	Dolomite	II	0.1847	5.325	0.1023	0.511875±9

Regression and age calculations of isochrons were performed using Isoplot/Ex Version 3.00 software (Ludwig, 2008). The ratio error of $^{147}Sm/^{144}Nd$ and $^{143}Nd/^{144}Nd$ is 1% and 0.03%, respectively. The carbonate minerals have yielded an isochron age of 211 ± 4 Ma (Figure 10a), with the value of mean square of weighted deviate (MSWD) 7.3 and the initial $^{143}Nd/^{144}Nd$ ratio 0.511731 ± 0.000009 (Figure 10a). The nonlinear relationship between the plots on the 1/Nd vs. $^{143}Nd/^{144}Nd$ diagram (Figure 10b) excludes the possibility of a mixing line. Thus, the Sm-Nd isochron age could represent the crystallization ages of the stage I carbonate minerals.

Preprints (www.preprints.org) | NOT PEER-REVIEWED | Posted: 11 January 2024 doi:10.20944/preprints202401.0877.v1

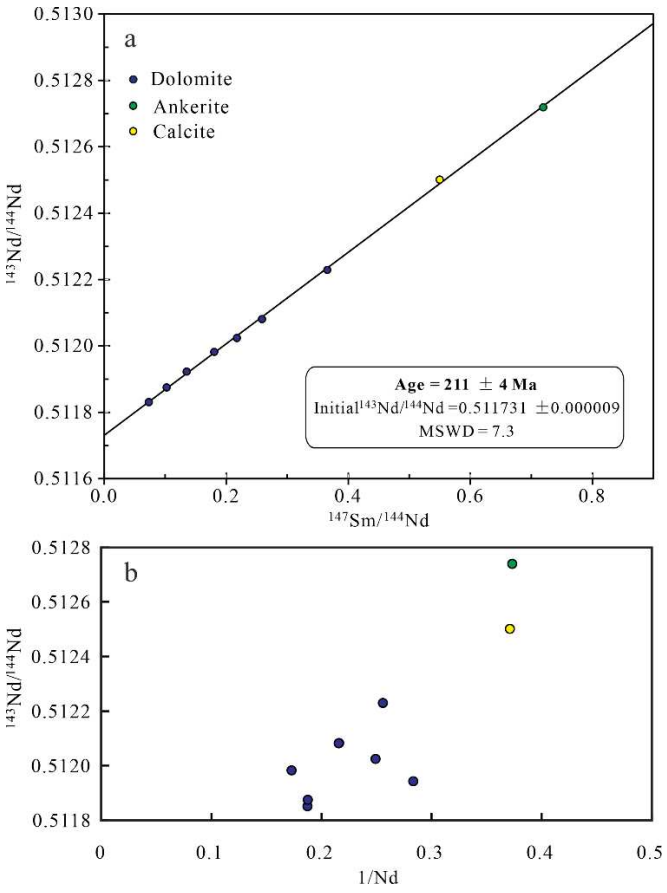

Figure 10. (a) Sm-Nd isochron age diagram of carbonates from the Dongtangzi Zn-Pb deposit; (b) Diagram of 1/Nd vs $^{143}Nd/^{144}Nd$.

6. Discussion

6.1. Sources of sulfur and metals

6.1.1. Source of sulfur

The sulfur isotopic compositions of sulfides extracted from mineral deposits traditionally serve as discerning indicators of sulfur sources, offering insights into ore formation conditions and genesis. Alterations in $\delta^{34}S$ values are commonly associated with shifts in source, temperature, pH, and oxygen fugacity (fO_2) (Ohmoto, 1972; Ohmoto and Rye, 1979; Wilkin and Barnes, 1996). The array of $\delta^{34}S$ values within a specific region furnishes valuable information regarding the dynamics of sulfide precipitation, sulfate reduction processes, the extent of isotopic fractionation, and discerns whether the fluid system was open or closed contingent on limited or unlimited sulfate supply (Jørgensen, 1979; Ohmoto and Rye, 1979; Ohmoto, 1992).

Many views about the sulfur source of Zn-Pb deposits in the Fengtai ore cluster have been proposed, such as, (1) a mixed source of reduced sulfur in seawater sulfate and sulfur in deep-sea hydrothermal fluids, by decomposition of metal sulfide complexes in hydrothermal fluids or the combination of metal chloride complexes in hydrothermal fluids with basinal H_2S (Wei and Lu, 1990); (2) a mixture of ^{32}S concentrated sulfur formed by biological reduction with sulfur extracted from the sulfate and sulfide in the sedimentary formation (Wang J.L., 1996); (3) the seawater sulfate mixed with the sulfur leached from the basement rock (Wang J.F., 1991; Ren et al., 2013). However, previous works has not separately studied different sulfides from different mineralization stages, with no in-situ analysis, which cannot avoid the mixing of sulfides from different stages and sources.

Using the most advanced in-situ LA-ICP-MS analysis method, this work obtained distinct sulfur isotopic compositions of sulfides from different mineralization stages. Pyrites in sedimentary period

Preprints (www.preprints.org) | NOT PEER-REVIEWED | Posted: 11 January 2024 doi:10.20944/preprints202401.0877.v1

have the highest positive $\delta^{34}S$ values (15.8‰~21.4‰), which are identical to Middle Devonian seawater sulfate (Claypool et al.,1980). The sulfides from the hydrothermal mineralization period have relatively uniform $\delta^{34}S$ values (1.1‰~10.2‰), peak values of +6 ~ +10‰ (Figure 11), obviously lower than that of the sedimentary period pyrite (15.8‰~21.4‰), partly overlapping that of the granite porphyry dike pyrite (2.1‰~4.3‰) (Table 2, Figure 11), suggesting that the sulfur of the hydrothermal mineralization period have a mixed source of magmatic sulfur and seawater sulfate, while the source of the sedimentary period sulfur is dominated by seawater sulfate. Wilkinson and Hitzman (2014) have advanced the hypothesis that magmatic heat, originating from the sub-crustal emplacement of mid-crustal sills, may serve as a catalyst for the regional fluid flow associated with Irish-type deposits. Similarly, Slack et al. (2015) have demonstrated that the ore-forming fluid of the black shale-hosted Red Dog Zn-Pb-Ag deposit emanated from hydrothermal fluids leached from mafic and ultramafic rocks at depth. Therefore, the contemporaneous magmatic activities at depth could have functioned as a primary or partial source of sulfur (S) for carbonate-hosted Pb-Zn deposits, including the Dongtangzi Zn-Pb deposit.

Compared with the pyrite from the hydrothermal mineralization period (averaging 7.2‰), the pyrite from the sedimentary period is remarkably rich in heavy sulfur (averaging 18.5‰), showing a seawater sulfate source, while the values of the pyrite of the granite porphyry dike (averaging 3.2‰) are closer to mantle-derived sulfur. The veined Stage I sphalerite in the siliceous rock range from 7.3 to 8.7‰ (sample D216.3), while the syngenetic disseminated pyrites from the siliceous rock are the most rich in heavy sulfur, ranging from 15.8 to 21.4‰ (sample D216.3), indicating that they have different sulfur sources and obviously do not reach isotopic equilibrium, even hosted in the same thin section. In general, if the $\delta^{34}S_{pyrite} > \delta^{34}S_{sphalerite} > \delta^{34}S_{galena}$, then the fractionation of S isotopes among minerals reached equilibrium (Zheng et al., 2000). The $\delta^{34}S$ values of the sulfides from the hydrothermal mineralization period show $\delta^{34}S_{sphalerite} > \delta^{34}S_{pyrite} > \delta^{34}S_{galena}$, displaying that the sphalerite and galena have reached equilibrium, but the pyrite and sphalerite have not, indicating that sulfur of the pyrite may be derived from a mixture of several sources.

Wang X. et al. (1996) obtained a range of 165-320°C for the homogenization temperature of the fluid inclusions in quartz and sphalerite from the main mineralization stage of the Dongtangzi Zn-Pb deposit. Usually, the TSR reaction at around 200°C will cause about 10‰ sulfur isotope fractionation between sulfates and reduced sulfurs (Kiyosu and Krouse, 1990; Machel et al., 1995). As the temperature increases, the degree of sulfur isotope fractionation caused by TSR (Thermochemical Sulfate Reduction) reaction gradually decreases, and there is generally no obvious sulfur isotope fractionation between sulfide minerals and reduced sulfur during mineral precipitation (Fry et al., 1986). Holser and Kaplan (1966) first proposed that the sulfur isotope values of seawater reached a minimum in the middle Devonian and then rapidly reached a maximum in the late Devonian (about 17‰ in the middle Devonian, about 30‰ in the late Devonian). The rapid increase in global seawater sulfur isotope values during the Devonian and early Triassic periods was possibly due to the rapid precipitation of pure sulfide minerals (Claypool et al., 1980).

If the sulfur in the Pb-Zn sulfides of the Dongtangzi deposit mainly comes from Devonian seawater sulfate, then the sulfur isotope composition range of sulfides formed by the TSR reaction of seawater sulfate at around 200°C would be the light blue area in Figure 11a, which is obviously higher than the sulfur isotope composition range of the measured sulfides in this study (Figure 11a, b). The single TSR process of Devonian seawater sulfate could not provide such low sulfur isotope composition, hence there must have involved a lot of light sulfur during mineralization processes. Possible sources include the following hypotheses: 1) Magmatic sulfur, as some of the Pb-Zn sulfides has consistent sulfur isotope compositions with pyrite in the granite porphyry dike (Figure 11) obtained in this study; 2) Sulfides enriched in light sulfur isotope through biogeochemical reduction reaction (BSR) of seawater sulfate during sedimentation, which is supported by the light sulfur isotope enriched pyrite ($\delta^{34}S<0$‰） in the wall rock of the Dongtangzi deposit (Figure 11a); 3) The seawater sulfate of the Triassic sedimentary basin distributed to the south of the Fengtai ore cluster is a potential sulfur source, as the Triassic seawater sulfate are relatively enriched in light sulfur isotope, that could potentially generate sulfides by TSR (Figure 11a, light blue area) with similar $\delta^{34}S$

Preprints (www.preprints.org) | NOT PEER-REVIEWED | Posted: 11 January 2024 doi:10.20944/preprints202401.0877.v1

range compared to the Pb-Zn sulfides of the Dongtangzi deposit (Figure 11a). During Middle Triassic, the west Qinling orogenic belt have experienced a rapid transformation from Yangtze-type stable shallow carbonate sedimentation to Tethys-type deep-sea thick turbidite sedimentation. The Tethys-type rift basin opened in middle Triassic, and rapidly closed in Middle Triassic to early Late Triassic, developing complexly folded deformation in the rigid massif, sandwiched between the two ancient blocks (Li Y.J., 2003). This rapid basin closure during Triassic may have created a suitable environment for the formation of evaporites, and the subsequent folding deformation provided the possibility of dissolution, infiltration, and long-distance transportation of the evaporites. For example, to the southeast of the Fengtai ore cluster, abundant evaporites are developed in the sedimentary rocks of the Middle Triassic Jialingjiang Formation in the northern margin of the Yangtze Block, adjacent to south Qinling belt, such as the Wadaozi, Huodigou and Zuoxigou gypsum deposits (Zheng et al., 1988; Yang et al., 2018).

In short, the sulfur associated with Zn-Pb mineralization of the Dongtangzi deposit has a mixed source of magmatic sulfur and seawater sulfate of evaporites from regional sedimentary formation.

6.1.2. Source of lead

Given the markedly diminished concentrations of thorium (Th) and uranium (U) in sulfide minerals, particularly in galena, the accrued influence of U and Th on radiogenic lead (Pb) isotopes within sulfides is deemed negligible, as attested by previous studies (Carr et al., 1995; Muchez et al., 2005; Pass et al., 2014). Consequently, the lead isotopic ratios derived from galena, sphalerite, and pyrite in the Dongtangzi deposit could represent the isotopic composition of the associated hydrothermal fluids.

Earlier studies suggested that metals of the Dongtangzi Zn-Pb deposit were originated from host Devonian to Carboniferous carbonate rocks (e.g. Wang, 1994; Zheng, 1994; Wang X. et al., 1996), and/or from magmatic activity in deep (Zhang et al., 2020). Li et al. (1999) suggested that Sinian to Carboniferous sedimentary rocks were important sources of metals. Wang et al. (1991) reported that the lead isotopic composition of the major deposits in Fengtai ore cluster (eg. The Qiandongshan, the Yindongliang, the Bafangshan, the Yinmusi, etc.) exhibited a relatively uniform and stable nature, with variations typically smaller than 1%. These findings indicated the presence of stable and normal lead with a high μ-value, suggesting a mixed source of lead originating from the crust within the orogenic belt. Qi et al. (1993) further noted that the sulfur and lead in the lead-zinc deposits of the Fengtai ore cluster originated from two distinct source regions, that is, the sulfur was derived from sea water while the lead is originated from the basement rock. Wang X. et al. (1996) proposed that the primary Pb-Zn source of the Pb-Zn deposits in the Fengtai ore cluster was the high-uranium crust rather than the mantle. This ore displayed characteristics of mixed lead, while the source region exhibited typical features associated with orogenic belts. Wang J.L. et al. (1996) further postulated that the initially enriched lead in ancient strata within the source region underwent leaching by subterranean hot water and was subsequently transported along growth faults to the seafloor, where mineralization occurred. The anomalous lead observed in the ore was attributed to the incorporation of crustal lead during later modification processes (Wang J.L. et al., 1996). However, prior investigations failed to differentiate sulfides from different mineralization stages and were not conducted in situ, resulting in the unavoidable mixing of lead from various stages and sources within the same sample.

In this study, the in-situ Pb isotope compositions of sulfides from different mineralization stages in the Dongtangzi deposit demonstrate a consistent and stable lead isotope composition across different hydrothermal mineralization stages. The narrow range of bulk isotopic data suggests a single source or else a well-mixed source of Pb (Table 3, Figure 12) (Zhou et al., 2018; Wei et al., 2020). However, the lead isotope composition of ore sulfides shows slight variations compared to the pyrite found in granite porphyry dikes, indicating some inconsistency in their source regions. That is, the ore sulfides are closer to the upper crust while the pyrite of the granite porphyry dikes are closer to orogenic belt (Figure 12a). This suggests that the primary source of lead-zinc elements may be from metamorphic basement rather than from magmatic sources. The lead isotope composition diagram

Preprints (www.preprints.org) | NOT PEER-REVIEWED | Posted: 11 January 2024 doi:10.20944/preprints202401.0877.v1

illustrates that ore sulfides of the Dongtangzi deposit and Triassic granitic rocks such as the Xiba intrusion in the West Qinling orogen (Figure 12) have similar lead isotope compositions, indicating that they may share the same source area. Meanwhile, the lead isotope compositions of ore sulfides partially overlap with those of the Neoproterozoic Yaolinghe Group and Bikou Group metamorphic basement (Figure 12) beneath the Fengtai ore cluster. Such Pb isotopic signatures rule out contributions of Pb from the Paleozoic Mianlue oceanic crust (Figure 12).

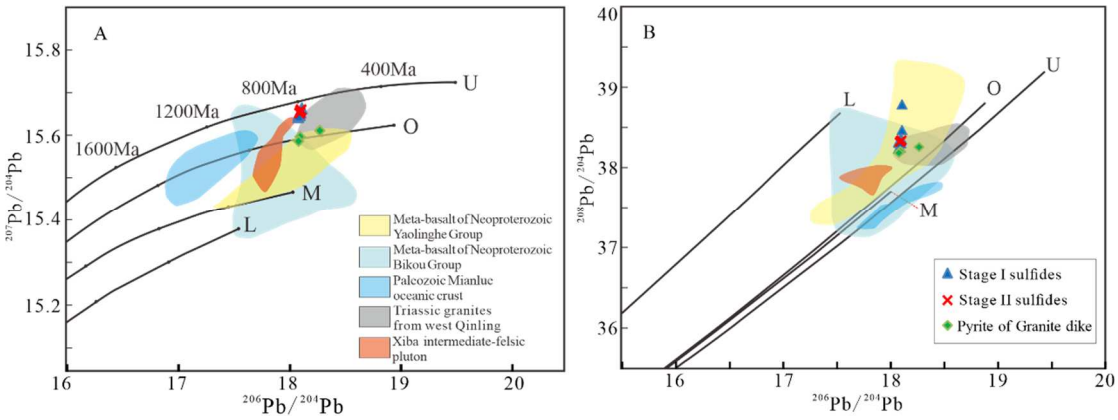

Figure 12. Comparison diagram of lead isotope of the Dongtangzi Pb-Zn deposit.

Trends for the upper crust (U), orogenic belt (O), mantle (M), and lower crust (L) are taken from Zartman and Doe (1981). Data for Triassic granites from the west Qinling orogenic belt from Zhang et al. (2006), Zhang et al. (2007a, b), Qin et al. (2007, 2008a, 200b, 2010); Neoproterozoic Yaolinghe and Bikou meta-volcanic rocks from Xia et al (2007, 2008); and Paleozoic Mianlue oceanic crust from Xu et al. (2002b).

These findings suggest that the metallic materials involved in ore formation originate from a mixture of Triassic magmatic processes and metamorphic basement. The remarkably homogeneous lead isotope composition of the ore sulfide (Table 3, Figure 12) mirrors that of global MVT or SEDEX-type lead-zinc deposits (Broadbent et al., 1998; Leach et al., 2005), indicating the thorough mixing of ore-forming fluids within the source region.

6.2. Timing of the ore formation

The isotope dating of ore minerals is the best method to determine the age of a hydrothermal deposit. Obtaining the age of associated gangue minerals can further determine the metallogenic age. Since different mineral phases have different chemical potential, the paragenetic minerals with different chemical properties precipitated from the same ore forming fluid may have different Rb/Sr values and Sm/Nd values. Consequently, for the dating of hydrothermal deposit, reliance on hydrothermal mineral assemblages proves more advantageous than exclusive reliance on a single mineral species (Liu et al., 1998; Liu X.L. et al., 2014). Sulfide Rb–Sr isochron dating method has been widely used for dating the sediment-hosted Pb-Zn deposits (Nakai et al., 1990, 1993; Zhang R.B. et al., 2008; Zhang C.Q., et al., 2008; Hu et al., 2012, 2015), as it could directly determine the age of a hydrothermal deposit. The calcium-bearing minerals such as calcite and fluorite in hydrothermal deposits are ideal objects for Sm-Nd isotopic dating (Halliday et al., 1990; Nie et al., 1999; Jiang et al., 2000). The temporal evolution of ore genesis within a hydrothermal deposit may span several million years, contrasting with a narrower timeframe of hundreds of thousands of years observed for a cohort of paragenetic hydrothermal minerals. Consequently, in the context of Rb–Sr isochron dating, it is reasonable to treat these paragenetic minerals as having formed synchronously (Liu et al., 1998). A similar situation also exists for the Sm-Nd isotopic system.

In this study, the handling of samples involved pulverizing sphalerite, galena, and pyrite single mineral particles to sizes below 200 mesh, followed by ultrasonic cleaning, effectively mitigating the interference from fluid inclusions within the minerals. Following the discriminant diagram proposed by Pettke et al. (1996), the constancy of the initial $^{87}Sr/^{86}Sr$ values during sulfide mineral growth can

Preprints (www.preprints.org) | NOT PEER-REVIEWED | Posted: 11 January 2024 doi:10.20944/preprints202401.0877.v1

be determined by utilizing 1/Rb-$^{87}Rb/^{86}Sr$ relation diagram, thus assessing the validity of the data. The 1/Rb-$^{87}Rb/^{86}Sr$ relation diagram (Figure 9b) demonstrate that the data points do not exhibit linear correlation. The Rb and Sr contents vary across distinct sphalerite, galena, and pyrite single mineral samples, while $^{87}Sr/^{86}Sr$ and $^{87}Rb/^{86}Sr$ values remain relatively stable. This observation indicates that the initial $^{87}Sr/^{86}Sr$ values of sphalerite, galena, and pyrite remain essentially unchanged during their growth, lending geological significance to the isochron ages derived, effectively representing the primary mineralization age. The fundamental premise of Sm-Nd isochron dating for hydrothermal minerals is homogeneity, contemporaneity, and closure of the isotopic system. To ensure the basic conditions of contemporaneity and homogeneity for all samples, in this study, the samples were carbonates associated with the ore sulfides of the main ore-forming stage (the mineralization Stage I and II). Additionally, there is no linear relationship between 1/Nd and ($^{143}Nd/^{144}Nd$) (Figure 11b), indicating that the isochron formed by the 9 data points (Figure 11a) has practical significance and could represent the primary ore-forming age.

The isochron ages of sulfides Rb-Sr (211.6 ± 2.6 Ma, Figure 10a) and carbonates Sm-Nd (211 ± 4 Ma, Figure 11a) are closely consistent within the error range, indicating that the main mineralization stage of the Dongtangzi Pb-Zn deposit occurred at about 211 Ma, that is, the Late Triassic.

The ages of some Zn-Pb and Au deposits in the Fengtai ore cluter have been reported, such as the Bafangshan-Erlihe Zn-Pb-Cu deposit has yielded a pyrite Re–Os isochron age of 226 ± 17 Ma (Zhang et al, 2011) and a sphalerite Rb–Sr isochron age of 220.7 ± 7.3 Ma (Hu et al., 2012). A quartz $^{40}Ar–^{39}Ar$ isochron age of 222.1 ± 3.5 Ma (Feng et al., 2003), a muscovite $^{40}Ar–^{39}Ar$ age of 209.5 ± 1.4 Ma, and Sm-Nd isochron ages of 209 ~ 208 Ma (Wang Y.T. et al., 2020b) have been obtained for the large Baguamiao gold deposit. A carbonate minerals Sm-Nd isochron age of 203.2 ± 1.6 Ma (Liu et al., 2014) and a sphalerite Rb-Sr isochron age of 210.2 ± 2.4 Ma (Wang Y.T. et al., 2018) for the Chaima gold deposit have been obtained. Wang et al. (2014) obtained a $^{40}Ar–^{39}Ar$ plateau age of 211.9 ± 1.5 Ma for sericite from the Simaoling gold deposit. In addition, to the west of the Fengtai ore cluster, the giant Changba-Lijiagou Pb-Zn deposit has a sulfide Rb-Sr isochron age of 222.3 ± 2.2 Ma (Hu et al, 2015). The large Liba gold deposit has yielded a mica $^{40}Ar–^{39}Ar$ age of 216.4 ± 1.5 Ma (Zeng et al., 2012).

Similar ages have been obtained from the igneous rocks of the Fengtai ore cluster, such as, the NWW-trending granite porphyry dike of the Dongtangzi deposit have yielded a zircon U-Pb age of 221.3 ± 1.4 Ma (Chen S.C. et al., 2020), the NE-trending diorite dikes crosscutting the main orebody of the Bafangshan-Erlihe deposit and the granite porphyry dike within the mine area have yielded zircon U-Pb ages of 221 ± 3 Ma (Zhang et al., 2011) and 217.9 ± 4.5 Ma (Wang et al., 2011a), respectively. The monzonitic granite and the granodiorite of the Xiba pluton (Figure 1c) yielded zircon U-Pb age of 219 ± 1 Ma, and 218 ± 1 Ma, respectively (Zhang et al., 2009). The ages of the Taibai pluton and the Baoji pluton to the north of the Fengtai ore cluster are 216 Ma (Zhang et al., 2006) and 216 to 210 Ma (Liu et al., 2011a), respectively. The main ages of the west Qinling magmatic belt are within a similar age range of approximately 220 Ma to 205 Ma (Sun et al., 2000; Chen, 2010; Qin et al., 2010). It is summarized that the ages of polymetallic deposits in west Qinling are ranging from 231 to 197 Ma, concentrated around 220 ~ 200 Ma; While the ages of the magmatic rocks are ranging from 248 to 195 Ma, concentrated around 230 ~ 200 Ma (Wang Y.T. et al., 2021).

The ages described above indicate that the Zn - Pb metallogenic events, magmatic activities and regional tectonic processes of west Qinling orogenic belt are consistent in time (Wang et al., 2009b; Mao et al., 2012) and were closely related to the post-collisional regional extensional regime between the Qinling micro-block and the Yangtze block along the Mianlue suture zone during Late Triassic - Middle Jurassic (Mao, 2001; Mao et al., 2002, 2012), belonging to the east Paleo-Tethys tectonic domain (Wang et al., 2014).

6.3. Ore genesis

As mentioned above, the M-shaped anticline structure hosting the Dongtangzi Zn-Pb deposit could be regarded as the first-order ore-controlling factor. Structural deformation, hydrothermal fracture-filling, hydrothermal replacement mineralization, and intensely wall-rock alteration

Preprints (www.preprints.org) | NOT PEER-REVIEWED | Posted: 11 January 2024 doi:10.20944/preprints202401.0877.v1

occurred after sedimentation and diagenesis. Additionally, the foreland basin environment that formed ore-hosting Devonian carbonate and clastic rocks (Dong et al, 2011, Dong and Santosh, 2016) is totally different from that of the SEDEX Pb-Zn deposits in the world, which formed in intra- and/or epicratonic rift and passive margin environments (Large et al., 2002; Leach et al., 2004, 2005). Therefore, Zn-Pb enrichment in this area should be dominated by epigenetic hydrothermal mineralization rather than syngenetic exhalative sedimentary processes.

Combining with the results of the Rb-Sr and Sm-Nd chronology and in-situ S-Pb isotopic studied in this work, the genesis of the Dongtangzi Zn-Pb deposit can be attributed to the multi-stage epigenetic hydrothermal fluid processes, driven by late Triassic regional tectono-magmatic activities. This work holds promising implications for understanding analogous Zn-Pb deposits of the west Qinling orogenic belt, given their similar geological settings and metallogenic characteristics.

7. Conclusions

1. The sulfur and Zn-Pb materials are believed to have originated from mixed sources of magmatic fluid and regional metamorphic basement.

2. The Dongtangzi Zn-Pb deposit is an epigenetic hydrothermal deposit, which formed in regional extensional regime during late Triassic, through epigenetic hydrothermal fluid processes.

Author Contributions: Investigation, Qiaoqing Hu, Yitian Wang, Shaocong Chen, Ran Wei, Xielu Liu, Changan Wang, Minjie Tang and Wentang Wu; data curation, Qiaoqing Hu, Yitian Wang, and Junchen Liu; writing—original draft preparation, Qiaoqing Hu, Yitian Wang; writing—review and editing, Yitian Wang and Qiaoqing Hu; project administration, Ruiting Wang and Weihong Gao. All authors have read and agreed to the published version of the manuscript.

Data Availability Statement: The data are derived from our team work or the references, and is available.

Acknowledgment: This Work was supported by the Ministry of Science and Technology of China (2016YFC0600106), the National Sciences Foundation of China (41372089), and the Fundamental Research Funds for the Central Public Welfare Research Institutes (K1607). We are grateful to the Baoji No.717 Corps Limited of Northwest Nonferrous Geological and Mining Group for their enthusiastic help with the field work.

Conflicts of Interest: All the authors declare no conflict of interest. The funders had no role in the design of the study; in the collection, analysis, or interpretation of data; in the writing of the manuscript; or in the decision to publish the results. In addition, co-authors Ruiting Wang, Weihong Gao, Changan Wang, Minjie Tang, and Wentang Wu are employees of the Northwest Nonferrous Geological and Mining Group Co., Ltd. The paper reflects the views of the scientists and not the company.

References

Bao, Z.A., Lu, C., Zong, C.l., Yuan, H.L., Chen, K.Y., Dai, M.N., 2017. Development of pressed sulfide powder tablets for in situ sulfur and lead isotope measurement using LA-MC-ICP-MS. International Journal of Mass Spectrometry 421, 255-262.

Broadbent, G.C., Myers, R.E., and Wright, J.V., 1998, Geology and origin of shale-hosted Zn-Pb-Ag mineralization at the Century deposit, northwest Queensland, Australia: Economic Geology, 93, 1264–1294.

Carr, G.R., Dean, J.A., Suppel, D.W., Heithersay, P.S., 1995. Precise lead isotope fingerprinting of hydrothermal activity associated with Ordovician to Carboniferous metallogenic events in the Lachlan fold belt of New South Wales. Economic Geology 90, 1467–1505.

Chen K Y, Yuan H L, Bao Z A. 2014. Accurate and precise in situ determination of lead isotope ratios in NIST, USGS, MPI-DING and CGSG reference glasses using femtosecond laser ablation MC-ICP-MS. Geostand Geoanal Res 38, 5–21.

Chen, S.C., Wang, Y.T., Yu, J.J., Hu, Q.Q., Zhang, J., Wang, R.T., Gao, W.H., Wang, C.A., 2020. Petrogenesis of Triassic granitoids in the Fengxian–Taibai ore cluster, Western Qinling Orogen, central China: Implications for tectonic evolution and polymetallic mineralization. Ore Geology Reviews 123, 103577.

Claypool, G.E., Holser, W.T., Kaplan, I.R., Hitoshi, S., Zak, I. 1980. The age curves of sulfur and oxygen isotopes in marine sulfate and their mutual interpretation. Chemical Geology, 28, 199–260.

Ding, T., Valkiers, S., Kipphardt, H., De Bievre, P., Taylor, P., Gonfiantini, R., Krouse, R., 2001. Calibrated sulfur isotope abundance ratios of three IAEA sulfur isotope reference materials and V-CDT with a reassessment of the atomic weight of sulfur. Geochimica Et Cosmochimica Acta. 65, 2433-2437.

Preprints (www.preprints.org) | NOT PEER-REVIEWED | Posted: 11 January 2024 doi:10.20944/preprints202401.0877.v1

Fang, W.X. 1997. Geochemical anomaly pattern and metallogenic model of the Bafangshan polymetallic deposit, Shaanxi. Geological exploration for non-ferrous metals, 6, 167–171 (in Chinese with English abstract).

Fang, W.X., 1999a. Reserch on mineral geochemistry of Qiandongshan Lead-Zinc deposit, a large-sized deposit in Fengxian County, Shaanxi. Acta Mineralogica Sinica, 19, 198-205 (in Chinese with English abstract).

Fang, W.X., 1999b. Characteristics of sedimentary facies of hydrothermal for the giant Qiantongshan Lead–zinc ore deposit, Feng County, Shanxi Province. Acta Sedimentologica Sinica, 17, 44-50 (in Chinese with English abstract).

Feng, J.Z., Wang, D.B., Wang, X.M., Shao, S.C., Ma, Z.G., Zhang, X.G. 2003. Geology and Metallogenesis of the Baguamiao Giant Gold Deposit in Fengxian, Shaanxi Province. Acta Geologica Sinica, 77, 387 – 398 (in Chinese with English abstract)

Fry, B., Gest, H., Hayes, J.M. 1986. Sulfur isotope effects associated with protonation of HS- and volatilization of H_2S. Chemical Geology, Isotope Geoscience section, 58, 253-258.

Fryer, B.J., Taylor, R.P. 1984. Sm-Nd direct dating of the Collins Bay hydrothermal uranium deposit, Saskatchewan. Geology, 12, 479-482.

Fu, J.L., Hu, Z.C., Zhang, W. 2016. In Situ Sulfur Isotopes ($\delta^{34}S$ and $\delta^{33}S$) Analyses in Sulfides and Elemental Sulfur Using High Sensitivity Cones Combined with the Addition of Nitrogen by Laser Ablation MC-ICP-MS. Analytica Chimica Acta, 911, 14-26.

Halliday, A.N., Shepherd, T.F., Dickin, A.P., Chesley, J.T., 1990. Sm-Nd evidence for the age and origin of a Mississippi Valley-type ore deposit. Nature, 344, 54–56.

Holser, W.T., Kaplan, I.R., 1966. Isotope geochemistry of sedimentary sulfates. Chemical Geology, 1, 93-135 (in: D.W. Kirkland and R. Evans. 1973. Marine Evaporites: Origin, Diagenesis, and Geochemistry. Dowden, Hutchinson and Ross, Stroudsburg, 374-398).

Hu, Q.Q., Wang, Y.T., Mao, J.W., Liu, X.L., Chen, S.C., Wei, R., Zhang, J., Wang, R.T., Wang, C.A., Dai, J.Z., Wen, S.W., Chen, M.S., 2020. Genesis of the Bafangshan-Erlihe Zn-Pb-Cu deposit in the Fengxian-Taibai ore cluster, west Qinling, China: Evidence from ore geology and ore-forming fluids. Ore Geology Reviews 126, 103734.

Hu, Q.Q., Wang, Y.T., Mao, J.W., Wei, R., Liu, S.Y., Ye, D.J., Yuan, Q.H., Dou, P., 2015a. Timing of the formation of the Changba–Lijiagou Pb–Zn ore deposit, Gansu Province, China: Evidence from Rb–Sr isotopic dating of sulfides. Journal of Asian Earth Sciences 103, 350–359.

Hu, Q.Q., 2015b. The Mineralization Features, Mechanism and Metallogenic Regularity of the Fengtai Pb-Zn Polymetallic Ore Cluster in West Qinling, China. Beijing: Chinese Academy of Geological Sciences, 1-147.

Huang, Z.Y., Lu, R.A., 2003. Zoning characteristics and index of primary geochemical anomalies in Qiandongshan Pb-Zn deposit Shaanxi Province, China. Geology and Prospecting, 39, 39-44 (in Chinese with English abstract).

Jørgensen, B.B., 1979. A theoretical model of the stable sulfur isotope distribution in marine sediments. Geochimica et Cosmochimica Acta 43, 363–374.

Kiyosu, Y., and Krouse, H.R., 1990, The role of organic acid in the abiogenic reduction of sulfate and the sulfur isotope effect: Geochemical Journal, 24, 21–27.

Leach, D.L., Sangster, D., Kelley, K., Large, R.R., Garven, G., Gutzmer, J., Walters, S., 2005. Sediment-hosted lead-zinc deposits: A global perspective. Economic Geology, 100, 561–607.

Leach, D.L., Marsh, E., Emsbo, P., Rombach, C., Kelley, K.D., Reynolds, J., Anthony, M., 2004. Nature of hydrothermal fluids at the shale-hosted Red Dog Zn-Pb-Ag deposits, Brooks Range, Alaska. Economic Geology, 99, 1449–1480.

Li, J.H., 2008. Analysis on ore-controlling factors and prospecting potential of the Baguamiao-type gold deposits in Fengtai area, Shaanxi. Mineral resources and geology, 22, 62 – 64 (in Chinese with English abstract).

Li, Q., Wang, B.Q., Ma, Z.G. Wang, X.H., 2007. Space-time Relationship of Gold Deposit to Lead-Zinc Deposit in Fengtai Ore Field in South Qinling. Journal of Earth Sciences and Environment, 29, 15–21 (in Chinese with English abstract).

Li, W.B., Huang, Z.L., Xu, D.R., Cheng, J., Xu, C., Guan, T., 2002. Rb-Sr Isotopic method on Zinc-Lead ore deposits: a review. Geotectonica et Metallogenia, 26, 436 – 441 (in Chinese with English abstract).

Li, H. 1986. Sulfides typomorphism and genesis of the Qiandongshan Pb-Zn deposit in Feng Country. Geology and Prospecting, 22, 36-41 (in Chinese).

Li, J.Z., He, D.R., Wu, J.M., 1992. The Qinling-type Lead and Zinc ore deposit. Acta Geologica Sinica, 66, 257-268.

Liu, J.M., Zhao, S.R., Shen, J., Jiang, N., Huo, W.G., 1998. Review on direct isotopic dating of hydrothermal ore-forming processes. Progress in geophysics, 13, 46 – 55 (in Chinese with English abstract).

Lu, R.S., Wei, H.M., 1992. Characteristics and Genesis of the Silicalites in Hot-Water Sedianentary Lead-Zinc Deposits in the Qinling Mountains. Acta Petrologica Et Mineralogica, 11, 14 – 21 (in Chinese with English abstract).

Ludwig, K. R., 2008. User's Manual for Isoplot 3.70. A Geochronological Toolkit for Microsoft Excel. Berkeley Geochronology Center Special Publication, 4, 1–74.

Preprints (www.preprints.org) | NOT PEER-REVIEWED | Posted: 11 January 2024 doi:10.20944/preprints202401.0877.v1

Machel, H.G., Krouse, H.R., Sassen, R., 1995. Products and distinguishing criteria of bacterial and thermochemical sulfate reduction. Applied Geochemistry, 10, 373-389.

Magnall, J.M., Gleeson, S.A., Paradis, S., 2015. The importance of silicous radiolarian-bearing mudstones in the formation of sediment- hosted Zn-Pb±Ba mineralization in the Selwyn basin, Yukon, Canada. Economic Geology, 110, 2139–2146.

Mao, J.W., 2001. Geology, distribution and classification of gold deposits in the Western Qinling Belt, Central China. Bulletin of Mineralogy, Petrology and Goechemistry, 20, 11 – 13.

Mao, J.W., Qiu, Y.M., Goldfarb, R.J., Zhang, Z.C., Ren, F.S., 2002. Geology, distribution, and classification of gold deposits in the Western Qinling belt, Central China. Mineral. Depos. 37, 352–377.

Mao, J.W., Zhou, Z.H., Feng, C.Y., Wang, Y.T., Zhang, C.Q., Peng, H.J., Yu, M., 2012. A preliminary study of the Triassic large-scale mineralization in China and its geodynamic setting. Geol. China 39, 1437–1471 (in Chinese with English abstract).

Moore, D.W., Young, L.E., Modene, J.S., and Plahuta, J.T., 1986, Geologic setting and genesis of the Red Dog zinc-lead-silver deposit, western Brooks Range, Alaska: Economic Geology, 81, 1696–1727.

Muchez, P., Heijlen, W., Banks, D., Blundell, D., Boni, M., Grandia, F., 2005. Extensional tectonics and the timing and formiation of basin-hosted deposit in Europe. Ore Geology Review, 27, 241–267.

Nakai, S., Halliday, A.N., Kesler, S.E., Jones, H.D., Kyle, J.R., Lane, T.E., 1993. Rb-Sr dating of sphalerites from Mississippi Valley (MVT) ore deposits. Geochimica et Cosmochimica Acta, 57, 417 – 427.

Nakai, S., Halliday, A.N., Kesler, S.E., Jones, H.D., 1990. Rb-Sr dating of sphalerites from Tennessee and the genesis of Mississippi Valley type ore deposits. Nature, 346, 354–357.

Nie, F.J., Bjorlykke, A.B., Nilsen, K.S., 1999. The origin of the Proterozoic Bidjovagge gold-copper deposit, Finnmark, Northern Norway, as deduced from rare earth element and Nd isotope evidences on calcites. Resource Geology, 49, 13-25.

Ohmoto, H., 1972. Systematics of sulfur and carbon isotopes in hydrothermal ore deposits. Economic Geology, 67, 551–578.

Ohmoto, H., 1992. Biogeochemistry of sulfur and the mechanisms of sulfide–sulfate mineralization in Archean oceans. In: Schidlowski, M., Golubic, S., Kimberley, M.M., Mckirdy, D.M., Trudinger, P.A. (Eds.), Early organic evolution: implications for mineral and energy resources. Springer, Berlin, 378–397.

Ohmoto, H., Rye, R.O., 1979. Isotopes of sulfur and carbon. In: Barnes, H.L. (Ed.), Geochemistry of Hydrothermal Ore Deposits. Wiley, New York, 509–567.

Pass, H.E., Cooken, D.R., Davidson, G., Maas, R., Dipple, G., Rees, C., Ferreira, L., Tayler, C., Deyell, C.L., 2014. Isotope geochemistry of the northeast zone, Mount Polley alkali Cu-Au-Ag porphyry deposit, British Columbia: A case for carbonate assimilation. Economic Geology, 109, 859–890.

Pettke, T., Diamond, L.W., 1996. Rb-Sr dating of sphalerite based fluid inclusion-host mineral isochrones: A certification of why it works. Economic Geology, 91, 951–956.

Qi, S.J., Li, Y., 1993. The types and ore-controlling factors of Lead-Zinc deposits in the Devonian metallogenic belt of Qinling Mountain. Geological Publishing House, 1 – 178 (in Chinese with English abstract).

Qin, J.F., Lai, S.C., Grapes, R., Diwu, C.R., Ju, Y.J., Li, Y.F., 2010. Origin of LateTriassic high-Mg adakitic granitoid rocks from the Dongjiangkou area, Qinling orogen, central China: Implications for subduction of continental crust. Lithos, 120, 347–367.

Qin, J.F., Lai, S.C., Li, Y.F., 2008a. Slab breakoff model for the Triassic post-collisional adakitic granitoids in the Qinling orogenic belt, central China: zircon U-Pb ages, geochemistry and Sr-Nd-Pb isotopic constraints. International Geology Review 50, 1080–1104.

Qin, J.F., Lai, S.C., Wang, J., Li, Y.F., 2008b. Zircon LA–ICP MS U–Pb age, Sr–Nd–Pb isotopic compositions and geochemistry of the Triassic Wulong granodiorite (South Qinling, Central China) and their petrogenesis significance. Acta Geogica Sinica, 82, 425–437.

Qin, J.F., Lai, S.C., Wang, J., Li, Y.F., 2007. The high–Mg# adakite–like tonalites from Xichahe, South Qinling: its petrogenesis and geological implication. International Geology Review, 49, 1145–1158.

Ren, P., Liang, T., Liu, K.L., Niu, L., Lu, L., Zhang, W.J., 2014. Geochemistry of Sulfur and Lead Isotopic Compositions of Sedex Lead-zinc Deposits in Fengtai Mineral Cluster Region of Qinling Mountains. Northwestern Geology, 47, 137-149 (in Chinese with English abstract).

Shi, Y.H., Wang, Y., Chen, B.L., Tan, R.W., Gao, Y., Shen, J.H., 2022. Characteristics of silicon-calcium surface ore-controlling in Fengtai ore-concentration areas, West Qinling Mountains: Examples from Qiandongshan Pb-Zn deposit. Geology in China, 49, 226-240 (in Chinese with English abstract).

Slack, J.F., Dumoulin, J.A., Schmidt, J.M., Young, L.E., and Rombach, C.S., 2004, Paleozoic sedimentary rocks in the Red Dog Zn-Pb-Ag district and vicinity, western Brooks Range, Alaska: Provenance, deposition, and metallogenic significance. Economic Geology, 99, 1385–1414.

Sun, W.D., Li, S.G., Ya, D.C., Li, Y.J., 2000. Zircon U-Pb dating of granitoids from South Qinling, Central China and their geological significance. Geochimica, 29, 209 – 216 (in Chinese with English abstract).

Tang, M.J., 2013. Metallogenic model of Qiandongshan Lead-Zinc Mine and analysis on prospecting potential in Fengtai Ore Field. Nonferrous Metals (Mining Section), 65, 23-28 (in Chinese with English abstract).

Preprints (www.preprints.org) | NOT PEER-REVIEWED | Posted: 11 January 2024 doi:10.20944/preprints202401.0877.v1

Wang, D.S., Wang, R.T., Dai, J.Z., Wang, C.A., Li, J.H., Chen, L.X., 2009. "Dual ore-controlling factors" characteristics of metallic seposits in the Qinling Orogenic Belt. Acta Geologica Sinica, 83, 1719 – 1729 (in Chinese with English abstract).

Wang, J.L., He, B.C., Li, J.Z., He, D.R., 1996. Qinling-type Lead-Zinc ore deposits in China. Geological Publishing House, 116 – 145 (in Chinese with English abstract).

Wang, R.T. Wang, T., Gao, Z.J., Chen, E.H. Liu, L.X., 2007. The main metal deposits metallogenic series and exploration direction in Feng-Tai Ore Cluster Region, Shaanxi Province. Western Geology, 40, 77 – 84 (in Chinese with English abstract).

Wang, R.T., Li, F.L., Chen, E.H., Dai, J.Z., Wang, C.A., Xu, X.F., 2011. Geochemical characteristics and prediction of the Bafangshan-Erlihe large Lead-Zinc ore deposit, Feng country, Shaanxi province, China. Acta Petrologica Sinica, 27, 779 – 793 (in Chinese with English abstract).

Wang, X., Tang, R.Y., Li, S., Li, Y.X., Yang, M.J., Wang, D.S., Guo, J., Liu, P., Liu, R.D., Li, W.Q., 1996. Qinling orogeny and metallogenesis. Metallurgical Industry Press, 187 – 230 (in Chinese with English abstract).

Wang, Y.T., Hu, Q.Q., Wang, R.T., Gao, W.H., Chen, S.C., Wei, R., Wang, C.A., Wen, B., Wen, S.W., Tang, M.J., 2020a. A new metallogenic model and its significance in search for Zn-Pb deposits in Fengtai (Fengxian-Taibai) polymetallic ore concentration area, Shannxi Province. Mineral Deposits, 39, 587-606 (in Chinese with English abstract).

Wang, Y.T., Hu, Q.Q., Zhang, C.Q., Wang, R.T., Dai, J.Z., Li, J.H., Wang, C.A., Li, X., 2011. Geological evidence for epigenetic mineralization of the Bafangshan-Erlihe Pb-Zn-Cu deposit in the Fengxian-Taibai metallogenic zone, western Qinling belt, Central China. Let's Talk Ore Deposits, Proceedings of 11th SGA Biennial Meeting, 2011 Antofagasta, Chile, 743 – 744.

Wang, Y.T., Liu, X.L., Hu, Q.Q., Zhang, J., Chen, S.C., Wang, R.T., Dai, J.Z., Gao, W.H., Wen, S.W., Chen, M.S., Zhang, G.L., 2018. Rb-Sr isotopic Dating of Vein-like Sphalerites from the Chaima Au Deposit in Fengxian-Taibai Ore-concentration Area,Shaanxi Province and Its Geological Significance. Northwestern Geology, 51, 121-132 (in Chinese with English abstract).

Wang, Y.T., Mao, J.W., Hu, Q.Q., Wei, R., Chen, S.C., 2021. Characteristics and Metallogeny of Triassic polymetallic mineralization in Xicheng and Fengtai ore cluster zones, west Qinling, China and their implications for prospecting targets. Journal of Earth Sciences and Environment, 43, 409-435 (in Chinese with English abstract).

Wang, Y.T., Mao, J.W., Zhang, J., Wang, R.T., Chen, G.M., Hu, Q.Q., Chen, S.C., Liu, X.L., 2020b. Geochronological constraints on the Baguamiao gold deposit, West Qinling orogen, central China: Implications for ore genesis and geodynamic setting. Ore Geology Reviews, 122, 103508.

Wang, Y.T., Wang, R.T., Dai, J.Z., Li, J.H., Wang, C.A., Tian, M.M., Wen, B., 2009. The strike-slip duplex and its significance for mineralization in the Fengxian-Taibai ore area, western Qinling, central China. Acta Mineralogica Sinica, 29, 188 – 189 (in Chinese).

Wang, Y.T., Wang, R.T., Hu, Q.Q., Liu, S.Y., Wei, R., Li, J.H., Yuan, Q.H., Liu, X.L., Dai, J.Z.,Wen, S.W., Wang, S.Y., 2013. Comparison of Pb–Zn mineralization between the Fengxian–Taibai and the Xihe–Chengxian ore clusters in the western Qinling. Acta Mineralogica Sinica, 33, 52–54 (in Chinese).

Wang, Y.X., Yang, J.D., Chen, J., Zhang, K.J., Rao, W.B., 2007. The Sr and Nd isotopic variations of the Chinese Loess Plateau during the past 7Ma: Implications for the East Asian winter monsoon and source area of loess. Palaeogeography, Palaeoclimatology, Palaeoecology, 249, 351-361.

Wilkin, R.T., Barnes, H.L., 1996. Pyrite formation by reactions of iron monosulfides with dissolved inorganic and organic sulfur species. Geochim. Cosmochim. Acta 60, 4167–4179.

Wu, W.T., Yang, S.W., Wang, S.L., Wu, X.D., Chen, E.H., Zhang, X.G., 2015. Analysis of the Ore Controlling Factors and Prospecting Ideas of the Dongtongzi Lead and Zinc Mine. Gansu Metallurgy, 37, 65-70 (in Chinese with English abstract).

Wu, X.D., Song, S.K., Gao, W.H., Yang, S.W., Zhang, X.G., 2016. Geological Characteristics and Prospecting Direction of Lead-Zinc Mine in Shaanxi Qiandongshan-Dongtangzi. Gansu Metallurgy. 38, 87-94 (in Chinese with English abstract).

Xia, L.Q., Xia, Z.C., Li, X.M., Ma, Z.P., Xu, X.Y., 2008. Petrogenesis of the Yaolinghe group, Wudang group volcanic rocks and basic dyke swarms from eastern part of the South Qinling Mountains. Norwest Geology, 41, 1–29 (in Chinese with English abstract).

Xia, L.Q., Xia, Z.C., Xu, X.Y., Li, X.M., Ma, Z.P., 2007. Petrogenesis of the Bikou Group volcanic rocks. Earth Science Frontiers, 14, 84–101.

Xu, J.F., Castillo, P.R., Li, X.H., Yu, X.Y., Zhang, B.R., Han, Y.W., 2002. MORB-type rocks from the Paleo-Tethyan Mian-Lueyang northern ophiolite in the Qinling Mountains, central China: implications for the source of the low 206Pb/204Pb and high 143Nd/144Nd mantle component in the Indian Ocean. Earth and Planetary Science Letters 198, 323–337.

Yang, B. Tan, Y.T., 2018. Analysis of metallogenic regularity and prospecting potential of non-metallic minerals in Shaanxi Province. China Non-Metallic Minerals Industry, 132, 7-10 (in Chinese).

Preprints (www.preprints.org) | NOT PEER-REVIEWED | Posted: 11 January 2024 doi:10.20944/preprints202401.0877.v1

Yang, X.K., 1991. Comments on the genesis of the Qiandongshan Pb-Zn deposit in Fengtai area, Qinling. Northwest Geology, 4, 52-55 (in Chinese).

Yuan, H.L., Yin, C., Chen, K.Y., Bao, Z.A., Zong, C., Dai, M.N., Lai, S.C., Wang, R., Jiang, S.Y., 2015. High precision in-situ Pb isotopic analysis of sulfide minerals by femtosecond laser ablation multicollector inductively coupled plasma mass spectrometry. Science China Earth Sciences. 58, 1713-1721.

Zartman, R.E., Haines, S.M., 1981. The plumbotectonic model for Pb isotopic systematics among major terrestrial reservoirs—a case for bi-directional transport. Geochimica et Cosmochimica Acta, 52, 1327-1339.

Zhang F, Liu SW, Li QG, Wang ZQ, Han YG, Yang K and Wu FH. 2009. LA-ICP-MS zircon U-Pb geochronology and geological significance of Xiba Granitoids from Qinling,Central China. Acta Scientiarum Naturalium Universitatis Pekinensis, 45, 833 – 840 (in Chinese with English abstract).

Zhang, C.Q., Li, X.H., Yu, J.J., Mao, J.W., Chen, F.K., Li, H.M., 2008. Rb-Sr dating of single sphalerites from the Daliangzi Pb-Zn deposit, Sichuan, and its geological significances. Geological Review, 54, 532 – 538 (in Chinese with English abstract).

Zhang, F., Liu, S.W., Li, Q.G., Sun, Y.L., Wang, Z.Q., Yan, Q.R., Yan, Zhen., 2011. Re-Os and U-Pb Geochronology of the Erlihe Pb-Zn Deposit, Qinling orogenic belt, Central China, and constraints on is deposit genesis. Acta Geologica Sinica (English Edition), 85, 673 – 682.

Zhang, F.X., 1986. Characteristics and geological significance of the strawberry-like sulfide mineral in the lead-zinc deposit of Qiandongshan and Yinmusi in Shaanxi province. Geology and Prospecting, 22, 40-42.

Zhang, F.X., Wang, J.F., 1988. The submarine volcanic-exhalative-sedimentary origin of Lead-Zinc deposits in the Fengtai ore field, Shaanxi. Geological Review, 34(2): 157 – 168 (in Chinese with English abstract).

Zhang, G.L., Tian, T., Wang, R.T., Gao, W.H., Chang, Z.D., 2020. S, Pb isotopic composition of the Dongtangzi Pb−Zn deposit in the Fengtai ore concentration area of Shaanxi Province for tracing sources of ore−forming materials. Geology in China, 47, 472-484 (in Chinese with English abstract).

Zhang, G.L., Wang, R.T., Tian, T., Ding, K., Gao, W.H., Guo, W.W., 2018. Geological-geochemical Characteristics and Genesis of Dongtangzi Pb-Zn Deposit in Fengxian-Taibai Ore Concentration Area of Shaanxi,China. Journal of Earth Sciences and Environment, 40, 520-534 (in Chinese with English abstract).

Zhang, G.W., Cheng, S.Y., Guo, A.L., Dong, Y.P., Lai, S.C., Yao, A.P., 2004. Mianlue paleo-suture on the southern margin of the Central Orogenic System in Qinling-Dabie— with a discussion of the assembly of the main part of the continent of China. Geol. Bull. China. 23, 846–852 (in Chinese with English Abstract).

Zhang, H.F., Jin, L.L., Zhang, L., Harris, N., 2007a. Geochemical and Pb-Sr-Nd isotopic compositions of granitoids from western Qinling belt: constraints on basement nature and tectonic affinity. Science in China (Series D) 50, 184–196.

Zhang, H.F., Xiao, L., Zhang, L., 2007b. Geochemical and Pb–Sr–Nd isotopic compositions of Indosinian granitoids from the Bikou block, northwest of the Yangtze plate: constraints on petrogenesis, nature of deep crust and geodynamics. Science in China (Series D) 50 (7), 972–983.

Zhang, H.F., Zhang, L., Harris, N., Jin, L.L., 2006. U-Pb zircon ages, geochemical and isotopic compositions of granitoids in Songpan-Graze fold belt, eastern Tibetan Plateau: constraints on petrogenesis and tectonic evolution of the basement. Contributions to Mineralogy and Petrology 152, 75–88.

Zhang, R.B., Liu, J.M., Ye, J., Chen, F.K., 2008. Chalcopyrite Rb-Sr isochron age dating and it's ore-forming significance in Shouwangfen copper deposit, Hebei province. Acta Petrologica Sinica. 24, 1353 – 1358 (in Chinese with English abstract).

Zheng, W.Z., Cao, Z.Q., Wei, Z., Liu, Z.M., Xu, S.K., Deng, X.L., 1988. The characteristics, genesis and prospecting significance of "salt-soluble breccia" of Lower Middle Triassic in southern Shaanxi Province. Geology of Chemical Minerals, 2, 37-43 (in Chinese).

Zheng, Y.F., Chen, J.F., 2000. Steady Isotope Geochemistry. Beijing: Science Publishing House, 1-64 (in Chinese).

Zhu, Z.Y., Cook, N.J., Yang, T., Ciobanu, C.L., Zhao, K.D., Jiang, S.Y., 2016. Mapping of sulfur isotopes and trace elements in sulfides by LA-(MC)-ICP-MS: Potential analytical problems, improvements and implications. Minerals. 6, 14.

Zhu, Z.Y., Jiang, S.Y., Ciobanu, C.L., Yang, T., Cook, N.J., 2017. Sulfur isotope fractionation in pyrite during laser ablation: Implications for laser ablation multiple collector inductively coupled plasma mass spectrometry mapping. Chemical Geology, 450, 223-234.

Disclaimer/Publisher's Note: The statements, opinions and data contained in all publications are solely those of the individual author(s) and contributor(s) and not of MDPI and/or the editor(s). MDPI and/or the editor(s) disclaim responsibility for any injury to people or property resulting from any ideas, methods, instructions or products referred to in the content.